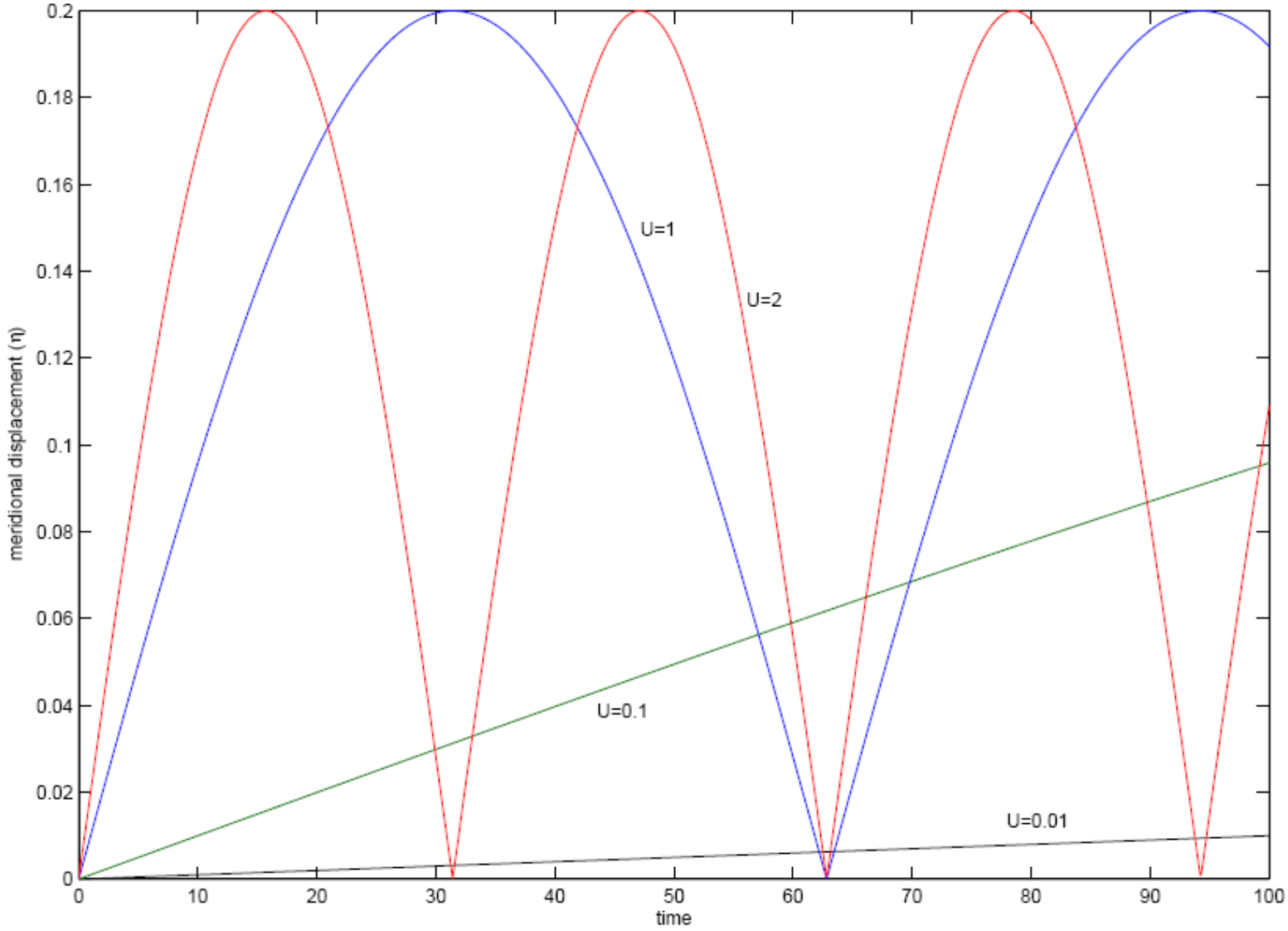

Meridional displacement as a function of U

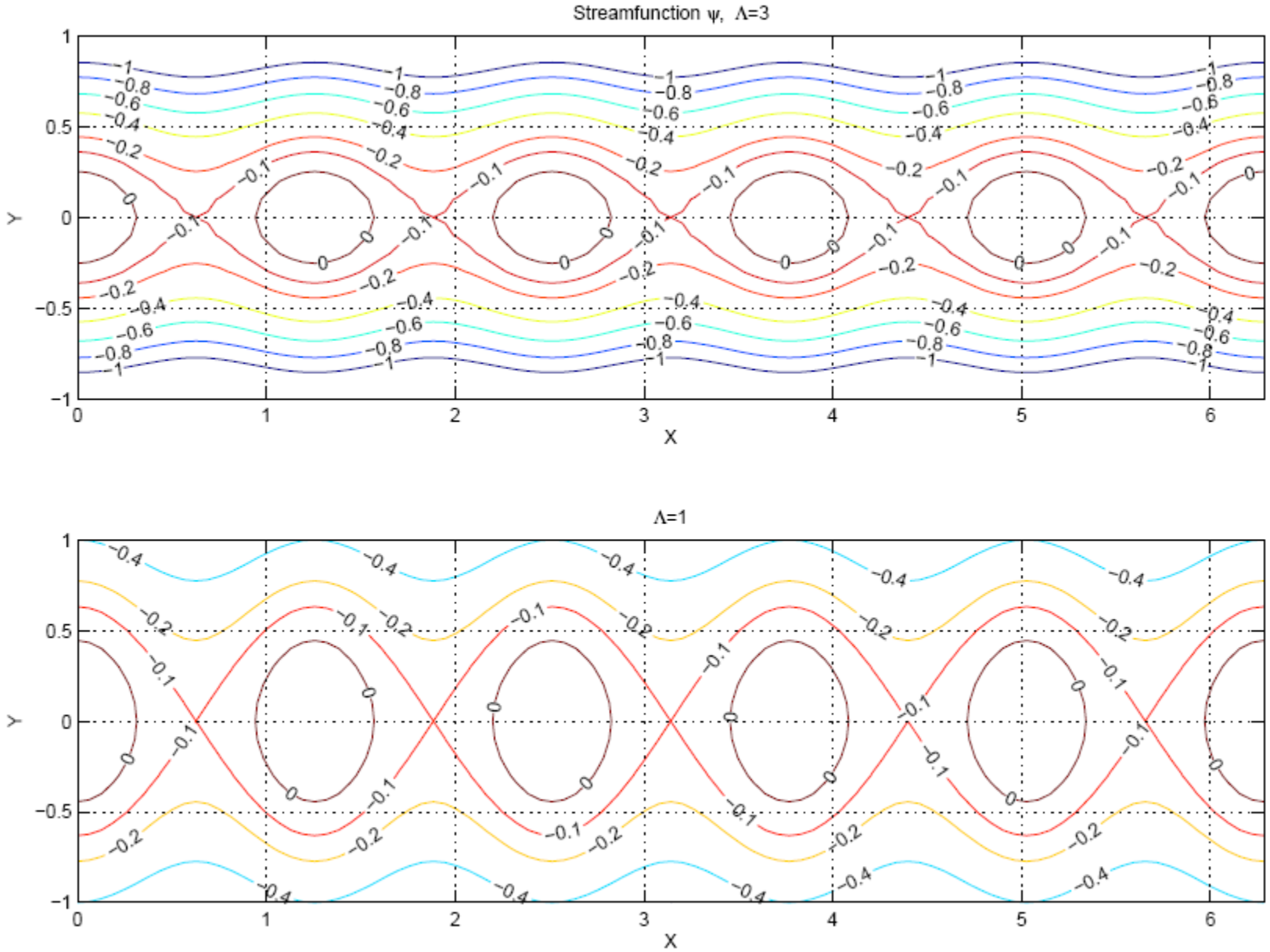

Streamfunction, for two values of constant meridional shear

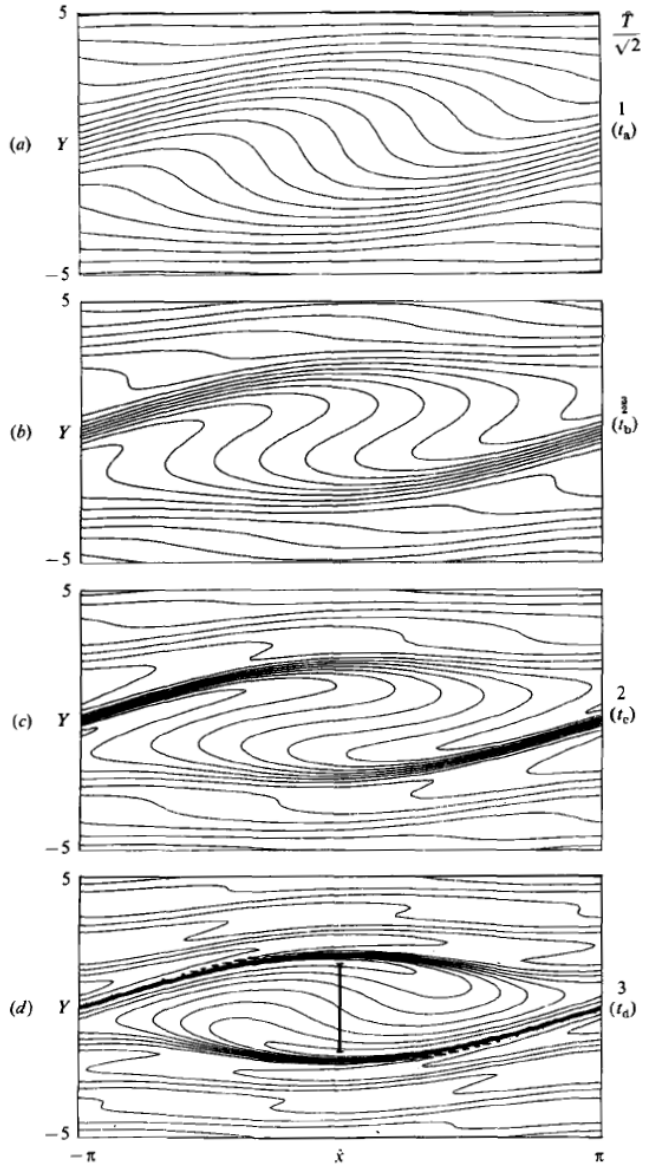

FIGURE 2. Contours of the absolute vorticity field predicted by the SWW analytical solution four times t_a, t_b, t_c and t_d. The dimensionless time units are the same as in figure 1; see also (2 Linear theory (Dickinson 1970) is beginning to break down at time t_a, panel (*a*), and pe reflection is attained just before time t_d, panel (*d*). The *y*-scale is exaggerated for clarity. The abs Y is expressed in units of Δy, where Δy is equal to $\epsilon^{\frac{1}{2}}A/\beta$, where $\beta = dq_0/dy$ is the basic abs (potential) vorticity gradient, and ϵ the disturbance amplitude defined in §2. The bar at the ce of (*d*) represents the 'mixing width' b, defined by equation (1.14).

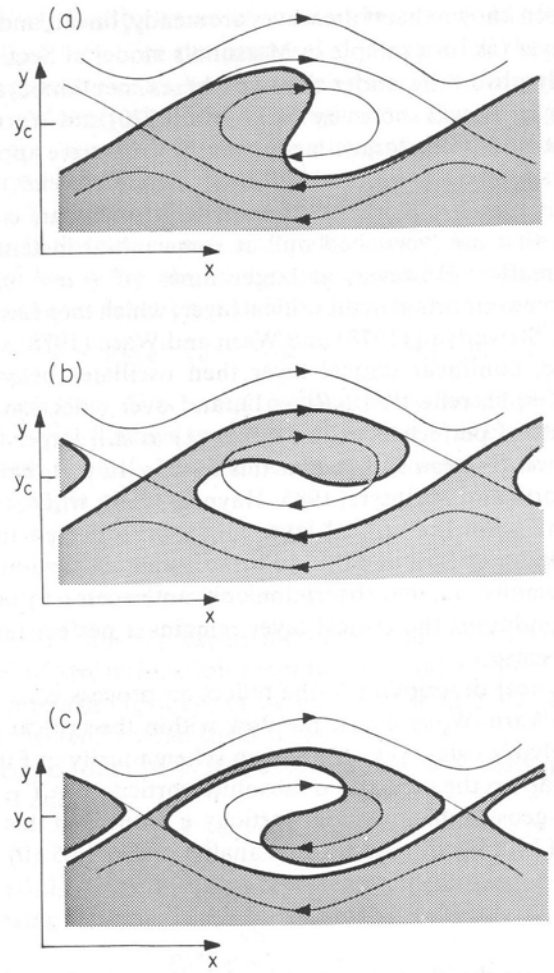

Fig. 5.13. Time-dependent analytical solution for a barotropic Rossby-wave nonlinear critical layer at non-dimensional times (a) $\alpha^{1/2}t^* = 2$, (b) $\alpha^{1/2}t^* = 4$, (c) $\alpha^{1/2}t^* = 6$ (Stewartson, 1978; Warn and Warn, 1978). The flow is periodic in x, and the y scale is greatly exaggerated: the initial critical line was at $y = y_c$. The thin lines indicate streamlines, and the "Kelvin's cats'-eyes" are the lens-shaped regions of closed streamlines; their width is of order $\alpha^{1/2}(y_1 - y_2)$. The thick line shows the successive positions of the material absolute vorticity contour, $\zeta = \zeta_c$ say, that initially lay along $y = y_c$. Thus $\zeta < \zeta_c$ in the stippled regions and $\zeta > \zeta_c$ in the unstippled regions. For this model, $\bar{v} \equiv 0$, so $v'\zeta' = v'\zeta = v'(\zeta - \zeta_c) = v(\zeta - \zeta_c)$. In (a) it can be seen that most of the stippled region within the cats'-eyes has $v > 0$, and most of the unstippled region has $v < 0$. Thus $v'\zeta' = v(\zeta - \zeta_c) < 0$ throughout most of the critical layer, Eq. (5.6.6) is negative, and $|R| < 1$ by Eq. (5.6.5), indicating partial absorption. Similar arguments show that in (b), $v'\zeta' \approx 0$ and $|R| \approx 1$, indicating near-perfect reflection, and in (c) $v'\zeta' > 0$ and $|R| > 1$, indicating overreflection. (Courtesy of P. H. Haynes.)

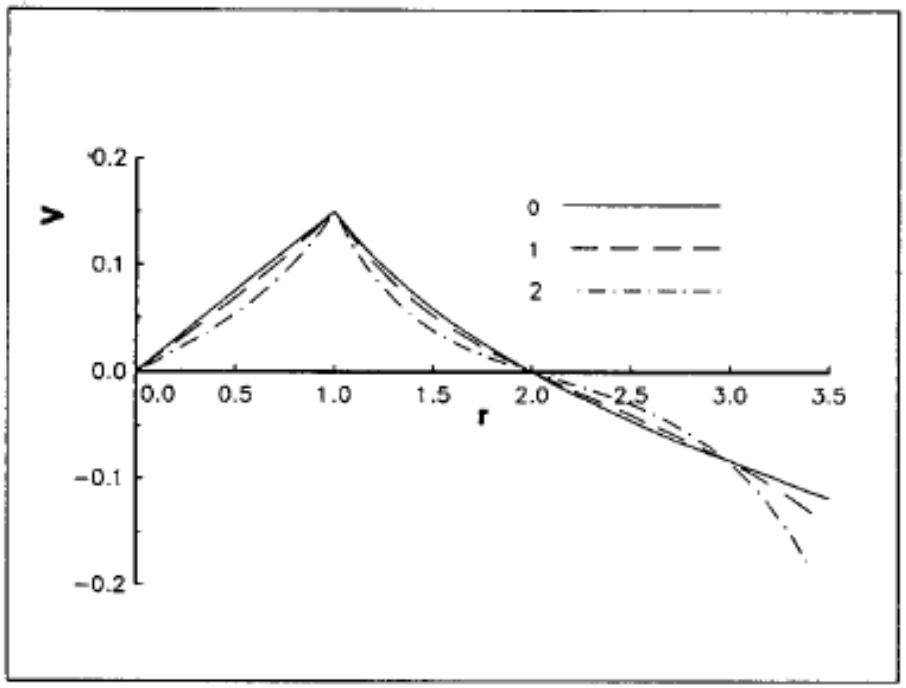
0.2
0.1
0.0
−0.1
−0.2
v
0.0
0.5
1.0
1.5
2.0
2.5
3.0
3.5
r
0
1
2

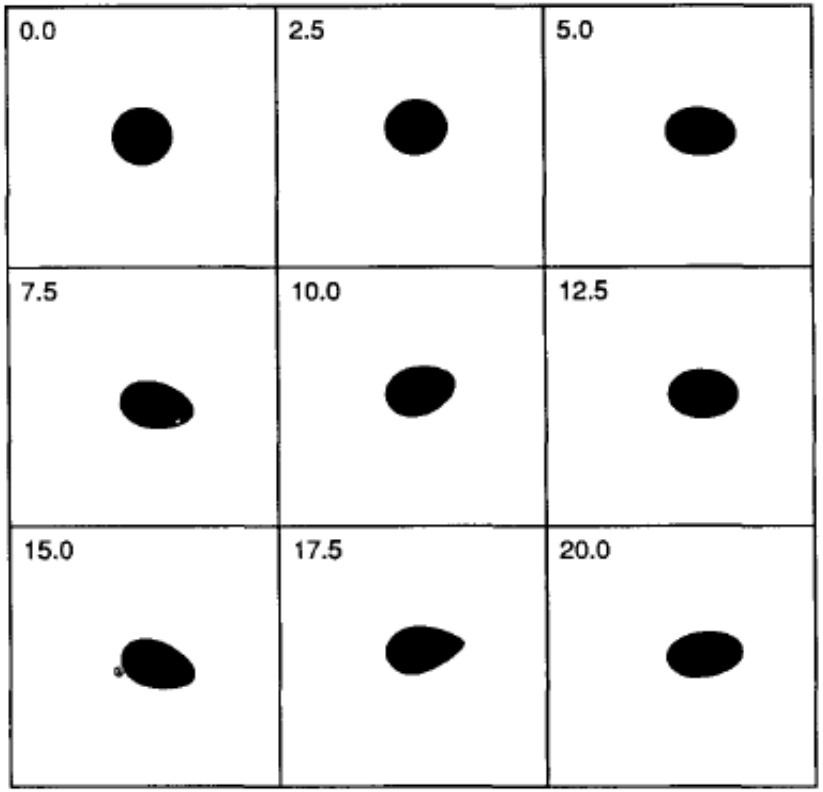

FIG. 2. Evolution of the vortex edge for the standard barotropic case ($\gamma = 0$) with $H_0 = 0.15$. Each box is centered on the coordinate origin (the center of the undisturbed vortex) which is indicated by the small cross. The numbers in the upper left-hand corner of each box gives the time in days.

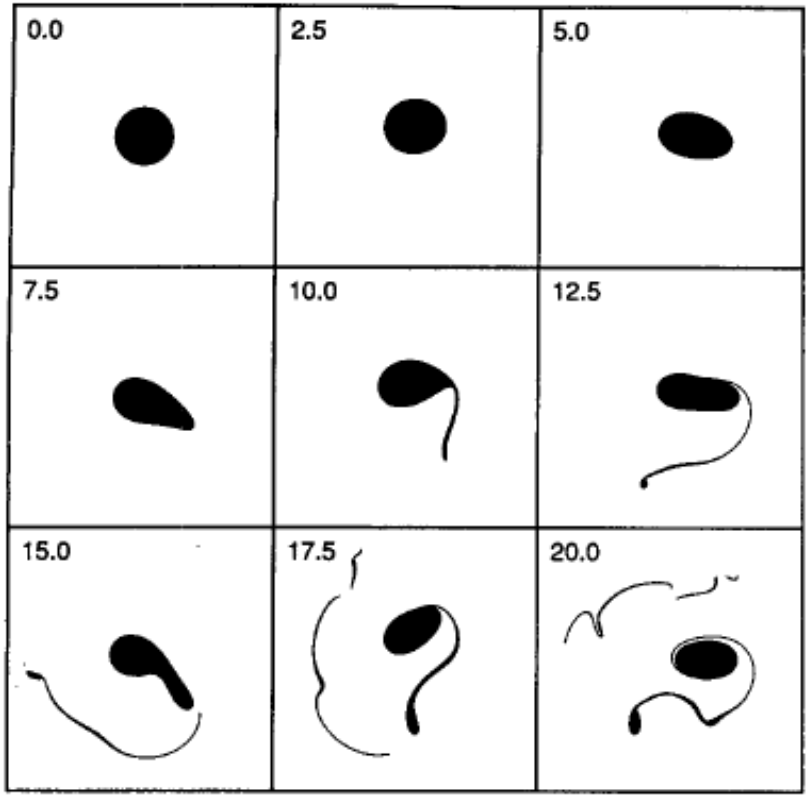

FIG. 3. As Fig. 2, but for larger forcing amplitude: $H_0 = 0.18$.

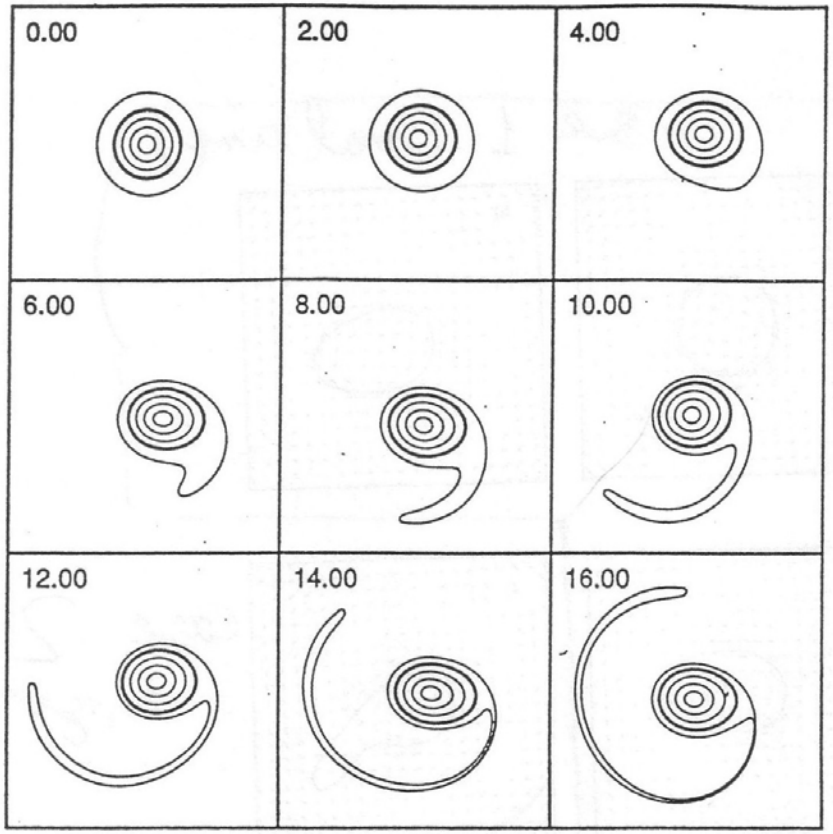
0.00
2.00
4.00
6.00
8.00
10.00
12.00
14.00
16.00

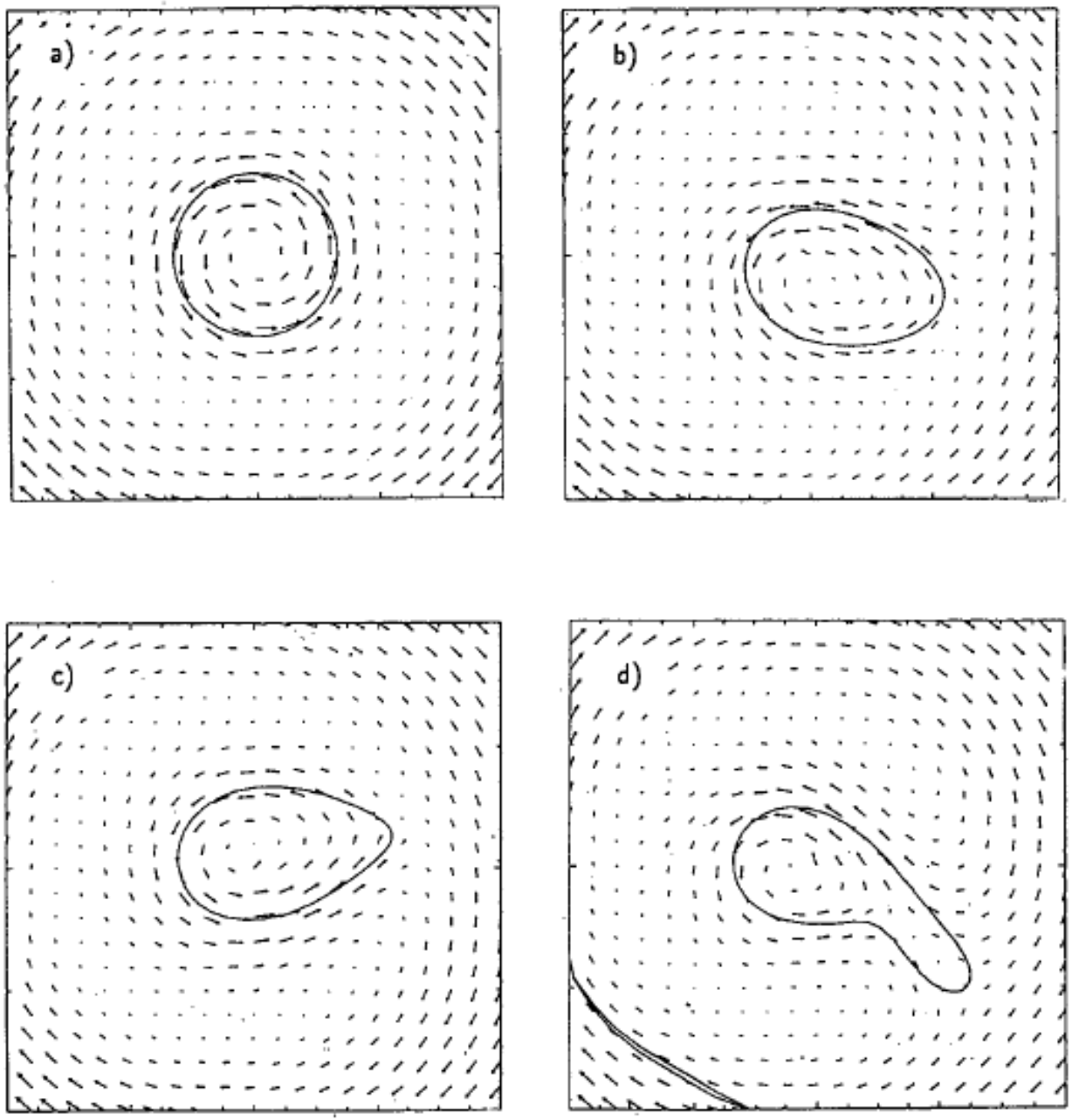

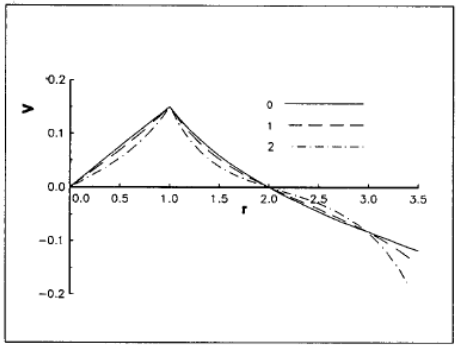

FIG. 7. The velocity field around the perturbed vortex for the case shown in Fig. 2: (a) the undisturbed vortex at $t = 0$; (b) the flow at $t = 7.5$d; (c) $t = 17.5$. (d) Flow at $t = 15$d for the case shown in Fig. 3. Note the location of the stagnation points.

Small breaking-micro-breaking

larger breaking

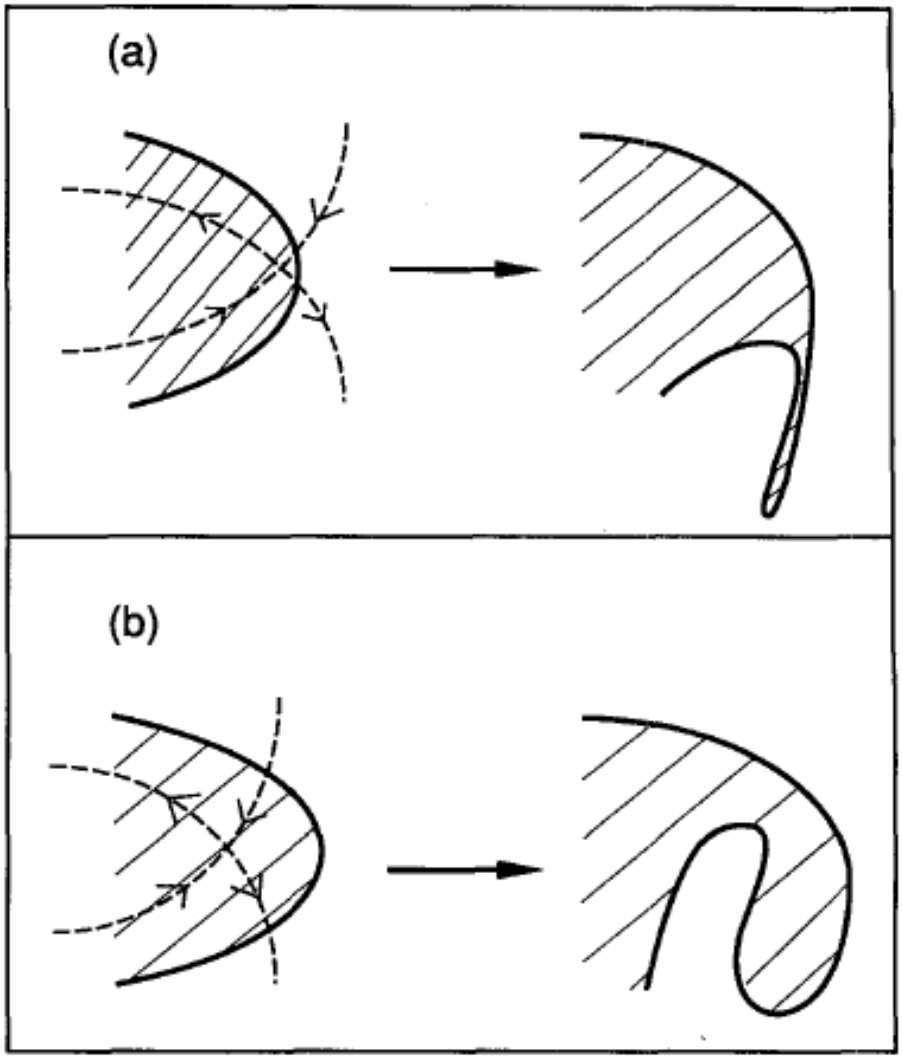

FIG. 11. Schematic illustrating the kinematics of wave breaking at the vortex edge. (a) Weakly supercritical case, with stagnation point close to vortex edge and ejection of a thin filament. (b) Strongly supercritical case with stagnation point well inside the vortex and ejection of a greater bulk of vortex material.

Fig. 2 Coarse-grain estimates of Ertel's potential vorticity Q on the 850 K isentropic surface (near the 10-mbar isobaric surface) on 17 (a) and 27 (b) January 1979, at 00 h GMT. The southernmost latitude circle shown is 20° N; the others are 30° N and 60° N. Map projection is polar stereographic. For units see equation (5) onwards. Contour interval is 2 units. Values greater than 4 units are lightly shaded, and greater than 6 units heavily shaded.

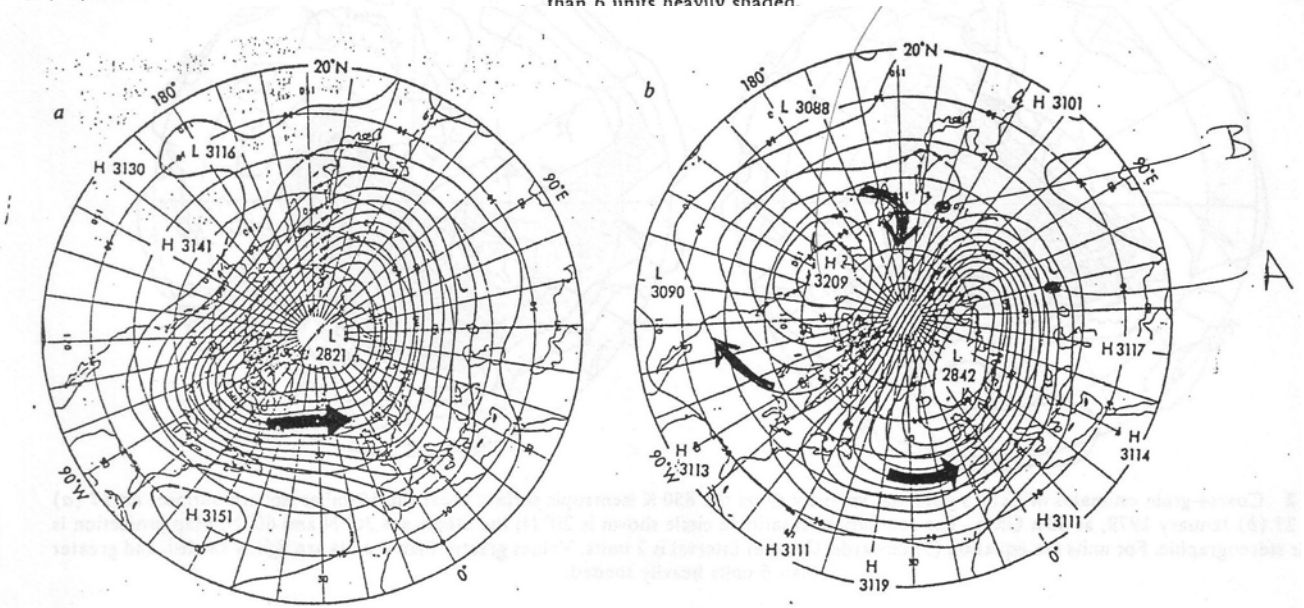

Fig. 1 Geopotential height in decametres (numerically nearly the geometric altitude above sea level) of the 10-mbar isobaric surface on 17 (a) and 27 (b) January 1979, at 00 h GMT. Contour interval is 24 decametres. Map projection is polar stereographic. The southernmost latitude circle shown is 20° N.

Observing breaking and filamentation- PV distribution fits wind fields

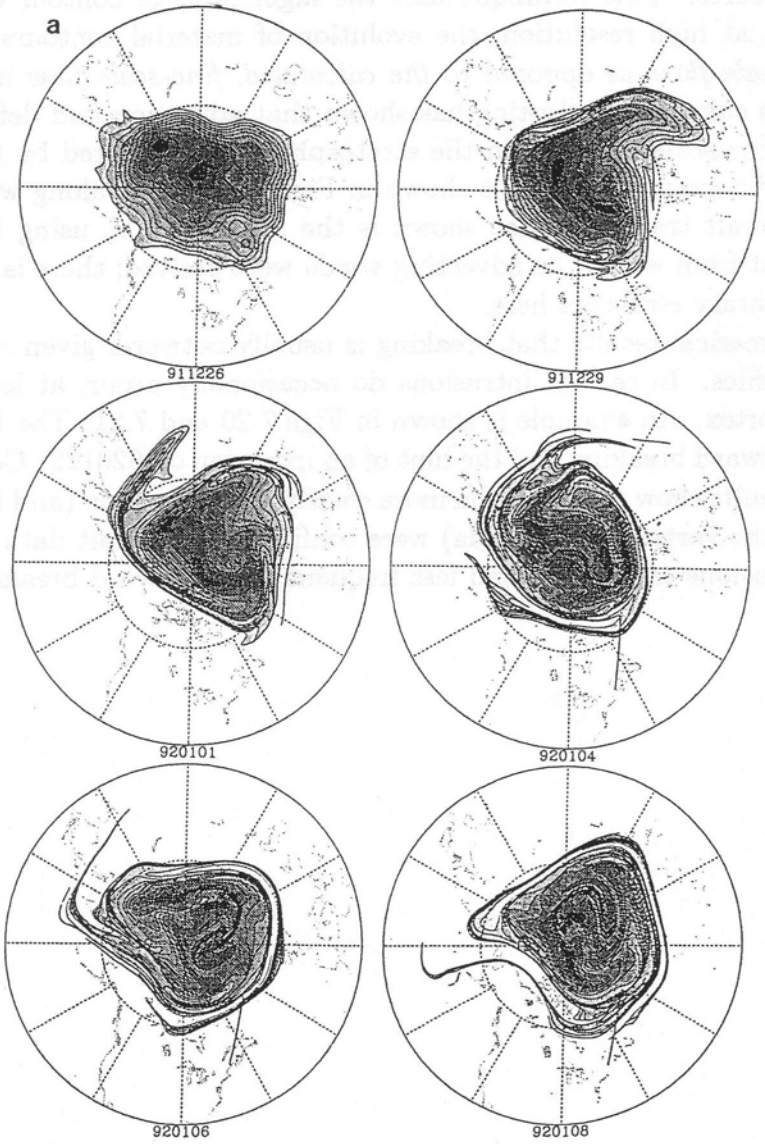

Figure 1. (a) Results of a CAS calculation from 1200 UT, December 26, 1991, using NMC-analyzed winds on the 450 K isentropic surface. The initial contours are put at the analyzed locations of the (20, 22, 24, $\cdots$) $\times 10^{-6}$ K m^2 s^{-1} kg^{-1} contours of Ertel PV on the 450 K surface. The ER-2 flight path is marked for the flights on January 4, 6, and 8. (b) Ertel PV on the 450 K surface from NMC analyses at 1200 UT on December 29, 1991, and January 1, 6, and 8, 1992. Contour levels are the same as in Figure 1a. North polar stereographic projections; 90°W is at bottom of figure.

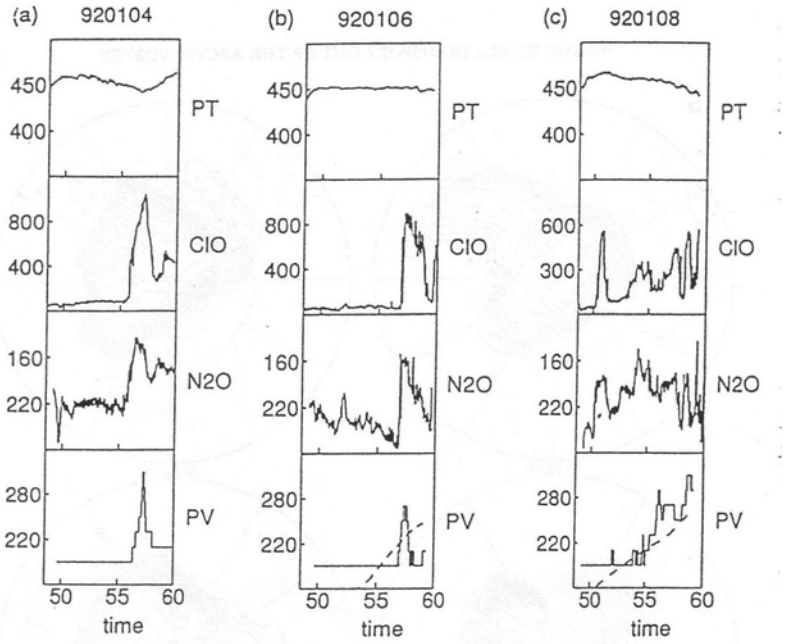

Figure 2. Data for northbound leg of ER-2 flights on (a) January 4, 1992; (b) January 6, 1992; and (c) January 8, 1992, as a function of universal time (kiloseconds). See Figure 1 for flight paths. Top to bottom: Potential temperature (K), ClO (parts per trillion by volume), and N_2O (parts per billion by volume) as measured aboard the ER-2; and PV from the CAS calculation (solid curve) and NMC analyses (dashed curve). PV is in units of 10^{-7} K m^2 s^{-1} kg^{-1}. Note that there are no NMC analyses on January 4, 1992.

Observing filamenation-tracers

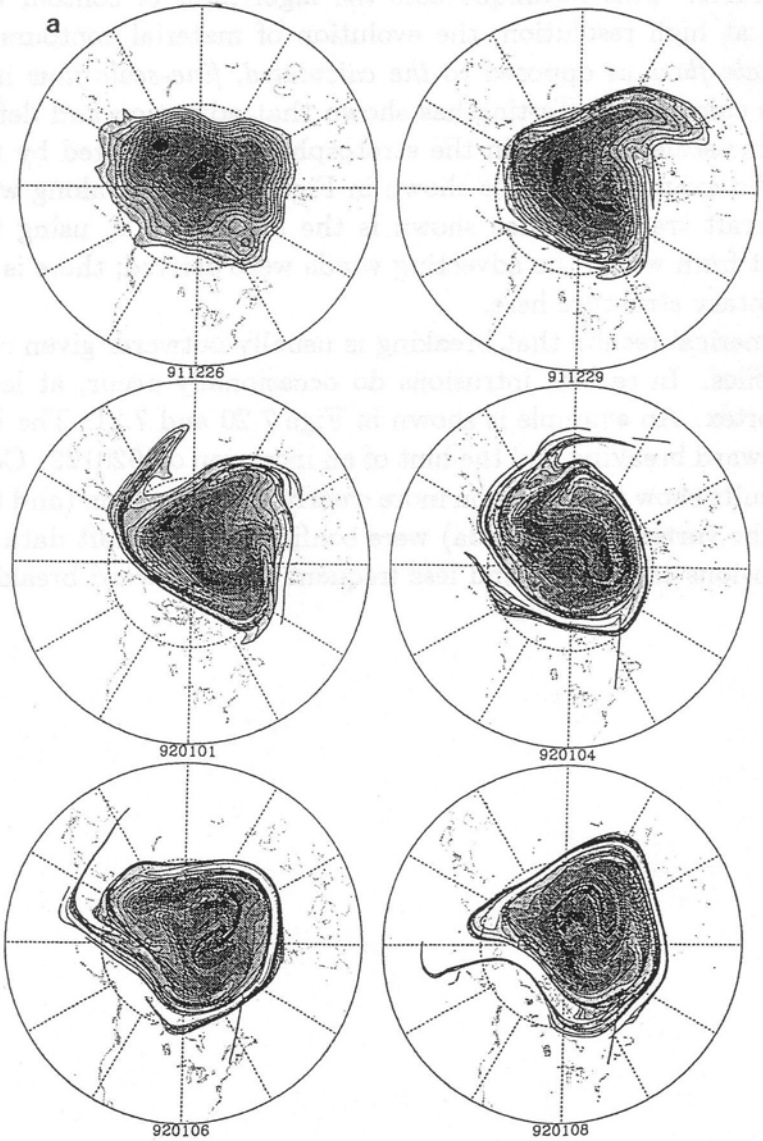

ure 1. (a) Results of a CAS calculation from 1200 UT, December 26, 1991, using NMC-analyzed nds on the 450 K isentropic surface. The initial contours are put at the analyzed locations of the (20, 22, ···) × 10^{-6} K m^2 s^{-1} kg^{-1} contours of Ertel PV on the 450 K surface. The ER-2 flight path is marked the flights on January 4, 6, and 8. (b) Ertel PV on the 450 K surface from NMC analyses at 1200 UT December 29, 1991, and January 1, 6, and 8, 1992. Contour levels are the same as in Figure 1a. North ar stereographic projections; 90°W is at bottom of figure.

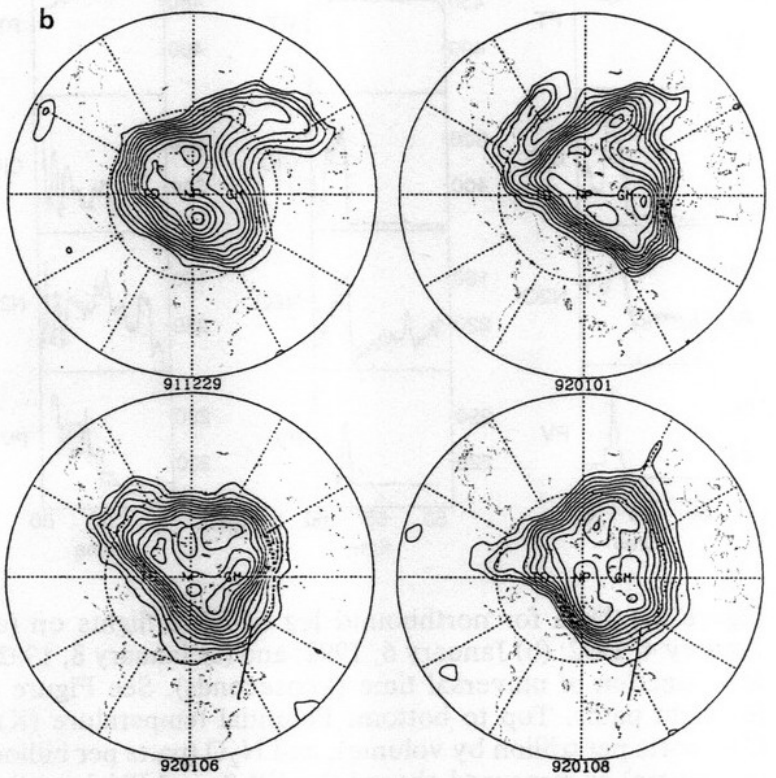

PV distribution in contour advection models vs observations

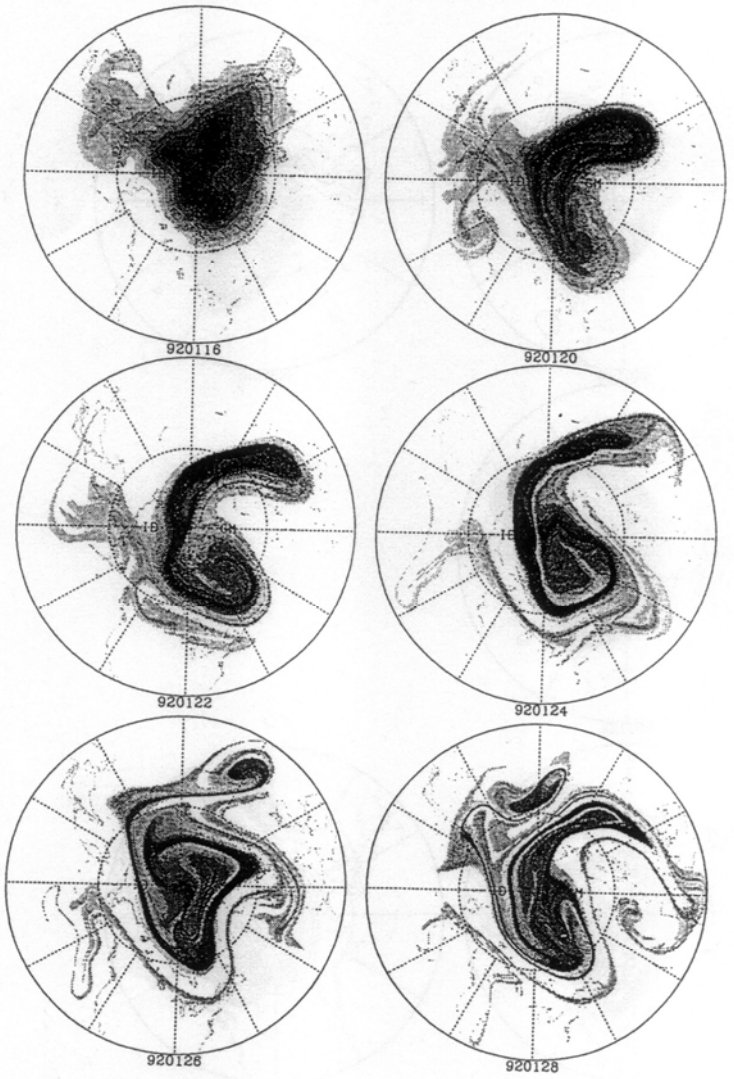

Figure 3. High-resolution evolution of the vortex on the 450 K isentropic surface, January 16–28, 199 as determined from CAS integrations. Material contours were initialized on January 16 at the location potential vorticity contours (2.0, 2.2, 2.4, 2.6 $\cdots$) $\times 10^{-5}$ K s^{-1} Pa^{-1} from the NMC analysis at that tim Subsequently, the contours were advected with the daily analyzed 450 K balanced winds.

Figure 7.21:

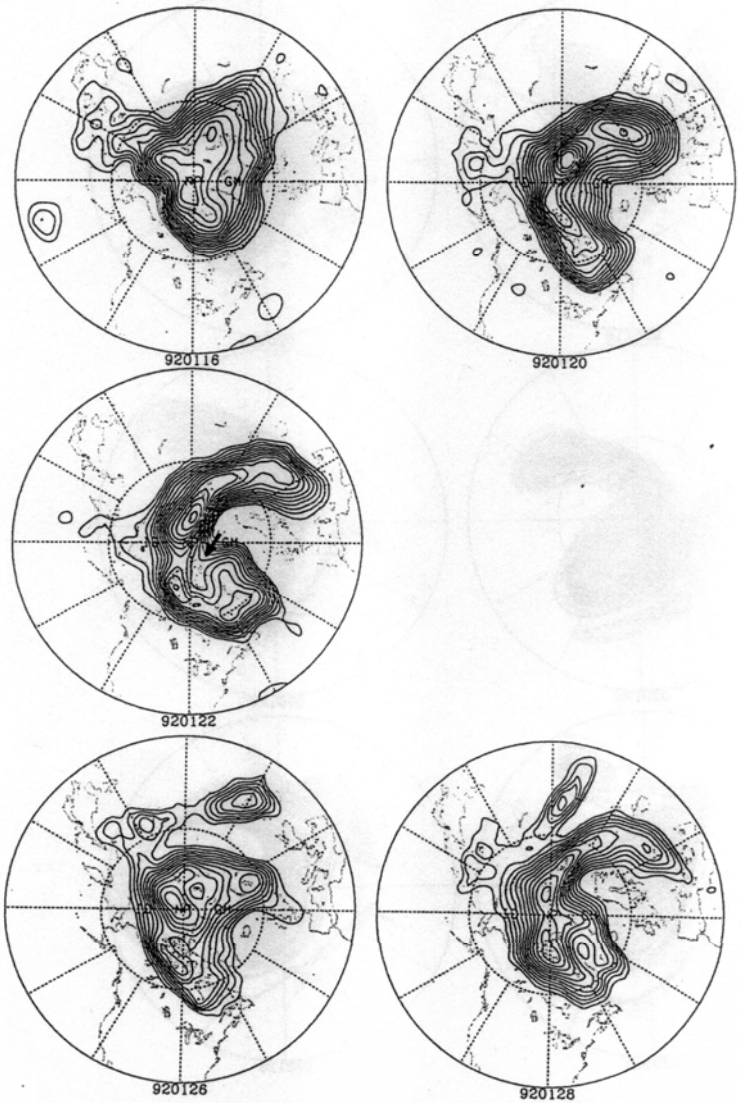

Figure 1. Ertel potential vorticity on the 450 K isentropic surface at 1200 UT for several days in the period January 16–28, 1992, from NMC analyses. (No data were available for January 24.) Contours are plotted every 2×10^{-6} K s^{-1} Pa^{-1}, beginning at 2×10^{-5} K s^{-1} Pa^{-1}. North polar stereographic projection; 90°W is at bottom of figure.

Figure 7.20:

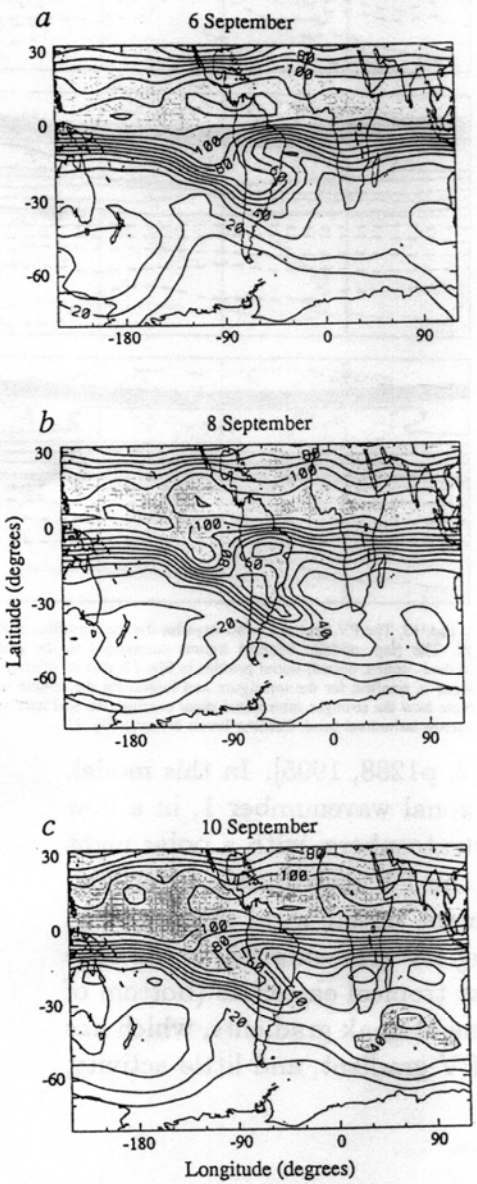

FIG. 2 a–c, Sequence of near-global maps of nitrous oxide (N_2O) mixing ratio (p.p.b.v.) on the 1,100 K isentropic surface for 6–10 September 1992. This isentropic level is near an altitude of 38 km, and close to a pressure surface of 5 hPa.

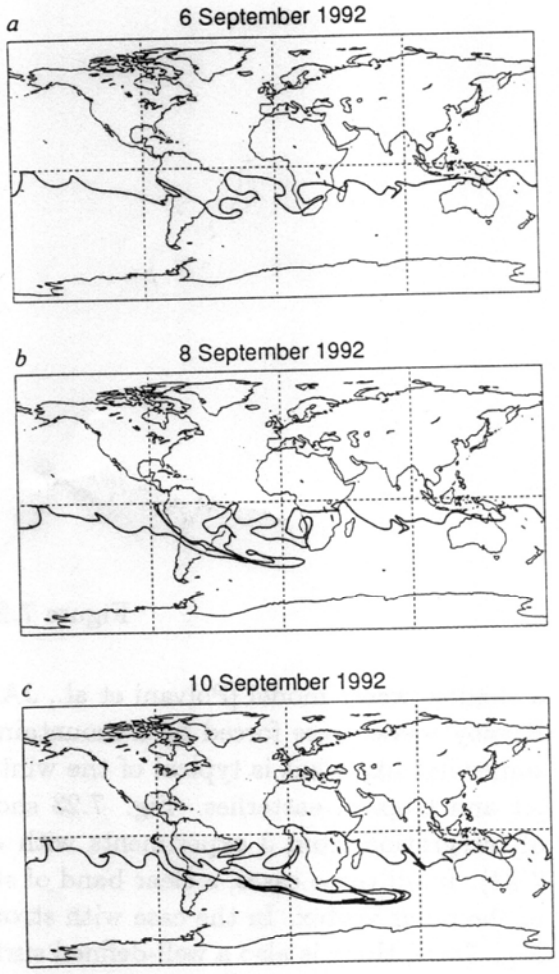

FIG. 1 a, b, c, Evolution of a material contour on the 1,100 K isentropic surface (approximate altitude 38 km and pressure 5 mb) for 6–10 September 1992, as determined by a CAS calculation. The calculation was started on 1 September 1992 at the 15° S latitude circle.

Chemical tracer distribution in contour advection models vs observations

7.22

Small vs large- depends on wave amplitude nd vortex structure.

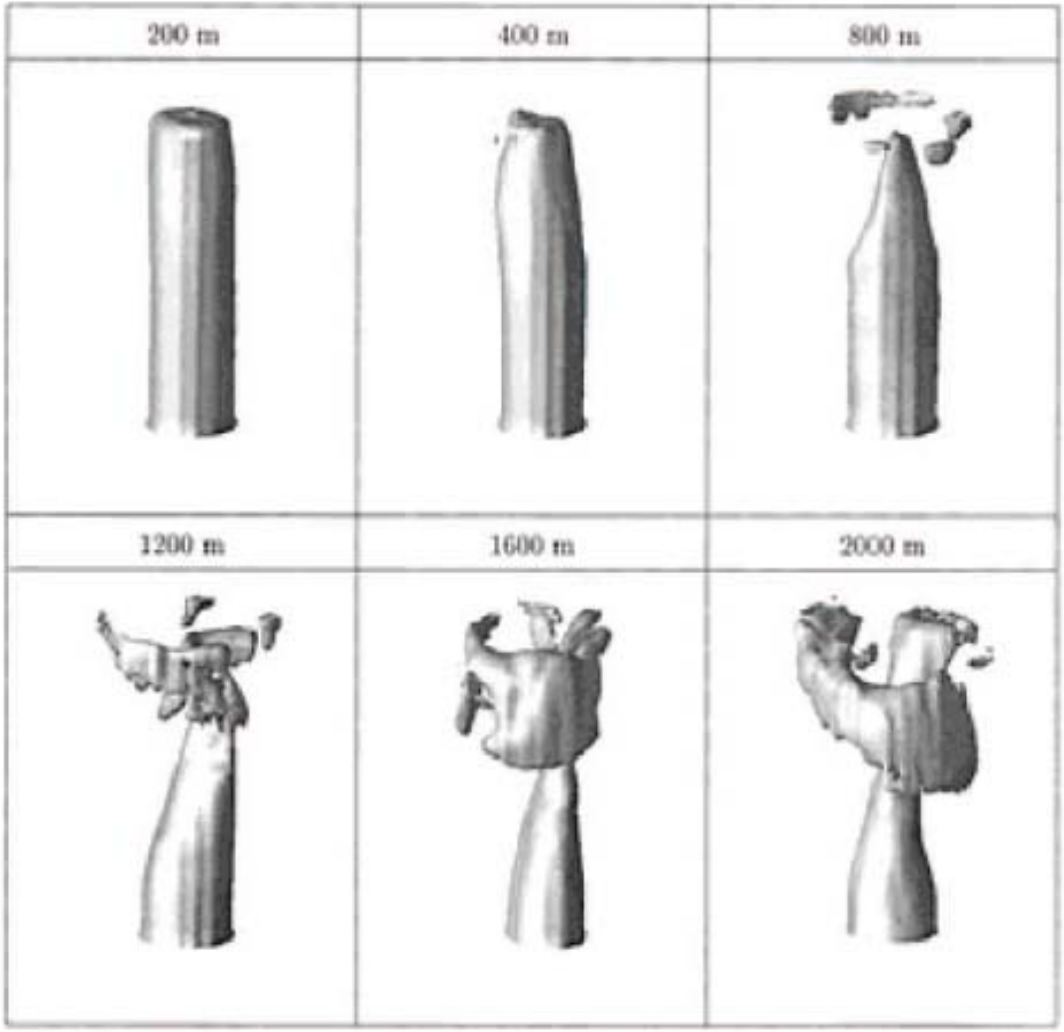

Polvani and Saravanan (2000)

$$n_{\text{ref}}^2 \equiv \frac{N^2}{f^2}\left[\frac{\overline{q}_y}{U} - k^2 + F(\rho, N^2)\right]$$

What happens first- $q_y<0$ or $U<0$?

$q_y<0$- reflection. Small breaking.
$U<0$- abosrption at a critical surface- large breaking

$$n_{\text{ref}}^2 \equiv \frac{N^2}{f^2}\left[\frac{\overline{q}_y}{U} - k^2 + F(\rho, N^2)\right] = m^2 + \frac{N^2}{f^2}l^2,$$

$$\overline{q}_y = \beta - U_{yy} + \frac{f^2}{N^2}\frac{U_z}{h} - \frac{f^2}{N^2}U_{zz} + f^2 U_z \frac{N_z^2}{(N^2)^2},$$

$$m^2 \approx \frac{N^2}{f^2}\beta + \frac{U_z}{h} - U_{zz}.$$

Northern hemisphere winter, SH during July-August: U_z matters most

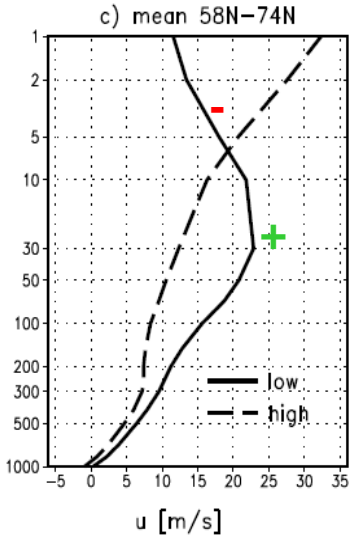

Observations for stationary wave 1: $U_z < 0$ in upper stratosphere reduces q_y near reflecting surface (5 mb).

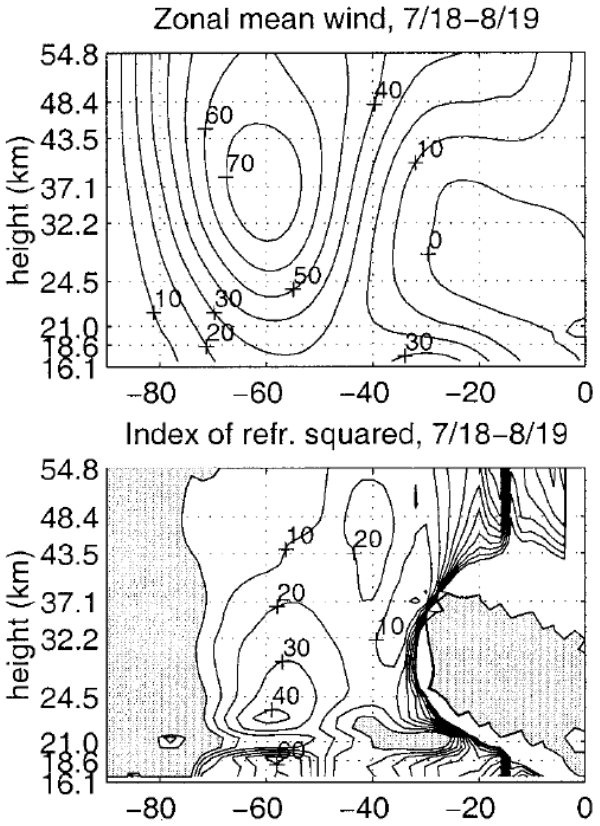

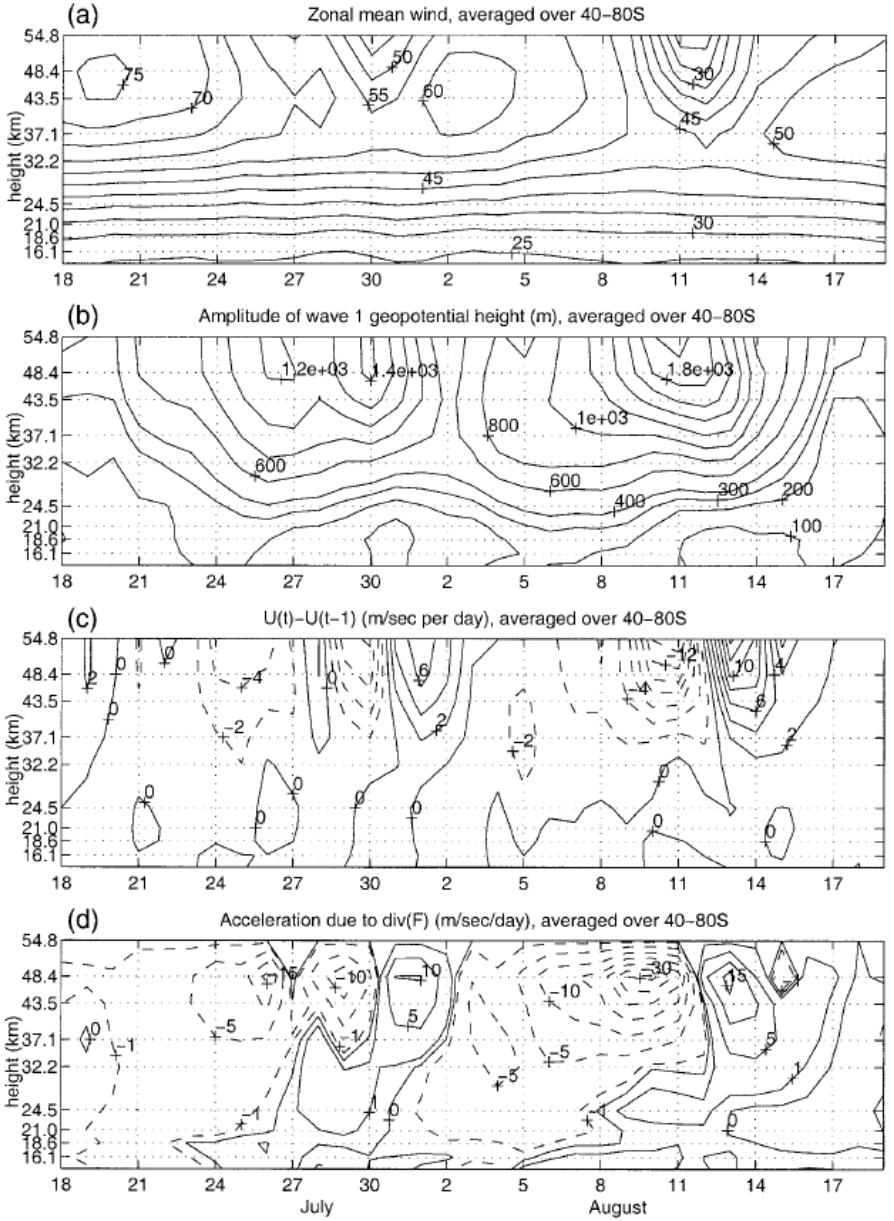

FIG. 6. Height–time sections (18 Jul–19 Aug 1996) of the 40°–80°S average of (a) zonal mean wind (contour interval of 5 m s^{-1}). (b) Wave 1 geopotential height amplitude (contours at 0, 100, and 200–2000, in jumps of 200 m). (c) The change in zonal mean wind over 1 day $[U(t) - U(t-1)]$. Contour interval is 2 m s^{-1}, negative values dashed. (d) The acceleration due to wave driving: $(\nabla \cdot \mathbf{F})/a_e\rho \cos\varphi$. Contours at ± 0, ± 1, and ± 5–30 in jumps of 5 m s^{-1} day^{-1}, negative values dashed. All quantities, except the wave geopotential height amplitude are volume averaged over latitude (weighted by $\cos\varphi$).

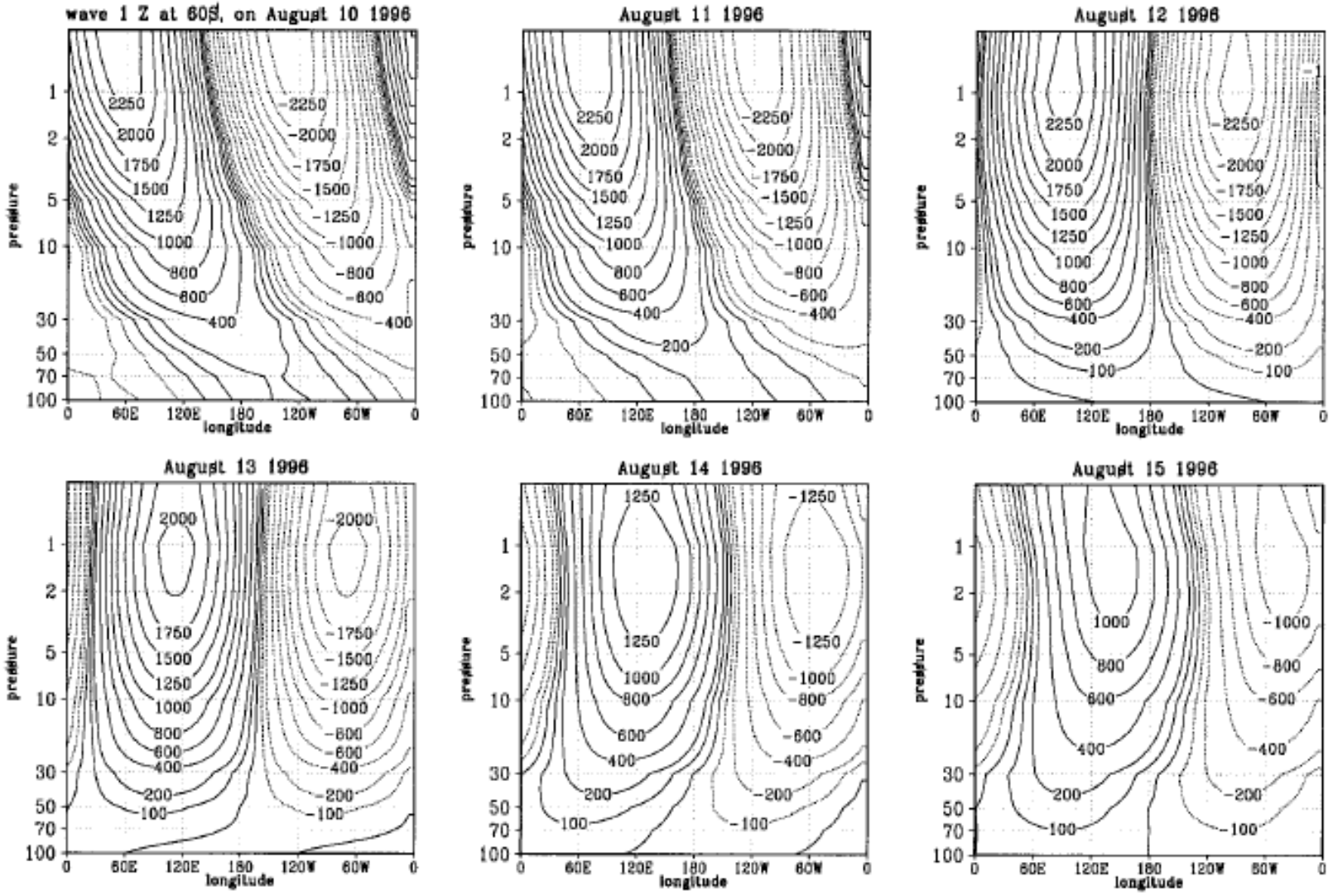

FIG. 7. Daily longitude–height cross sections at 60°S of wave 1 geopotential height for 10–15 Aug 1996. Contour intervals are at 0, ±100, ±200, ±400, ±600, ±800, and ±1000–2500, in jumps of 250 mb. Negative values are dashed. The vertical grid is the observational grid in millibars (100–0.4 mb).

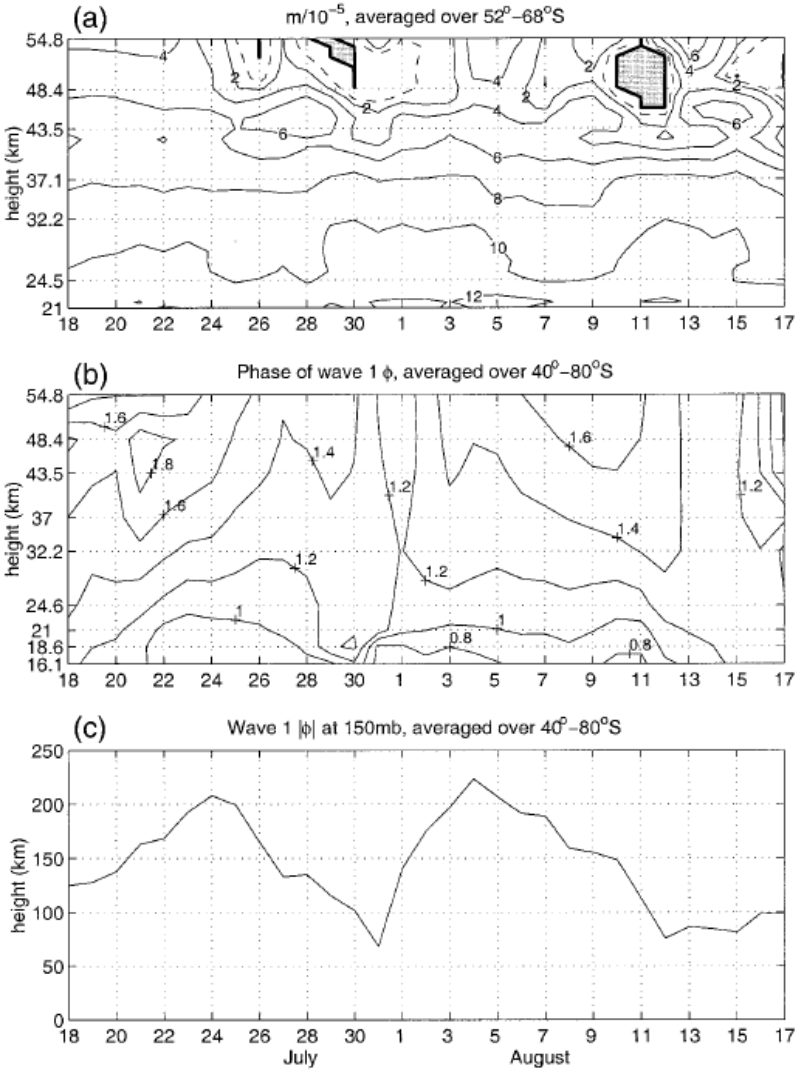

FIG. 10. Height–time sections (18 Jul–19 Aug 1996) of a latitudinal average of (a) vertical wavenumber m, calculated from the wave 1 steady-state solution to the daily observed basic state (10^{-5} m^{-1}). (b) The phase of wave 1 geopotential height (units of π). (c) The amplitude of wave 1 geopotential height at 150 mb (in m). Geopotential height quantities are averaged over 40°–80°S and m is averaged over 52°–68°S. Evanescent regions of m are shaded, and the thick and dashed lines denote values of 0.01 (the turning surface) and 1, respectively.

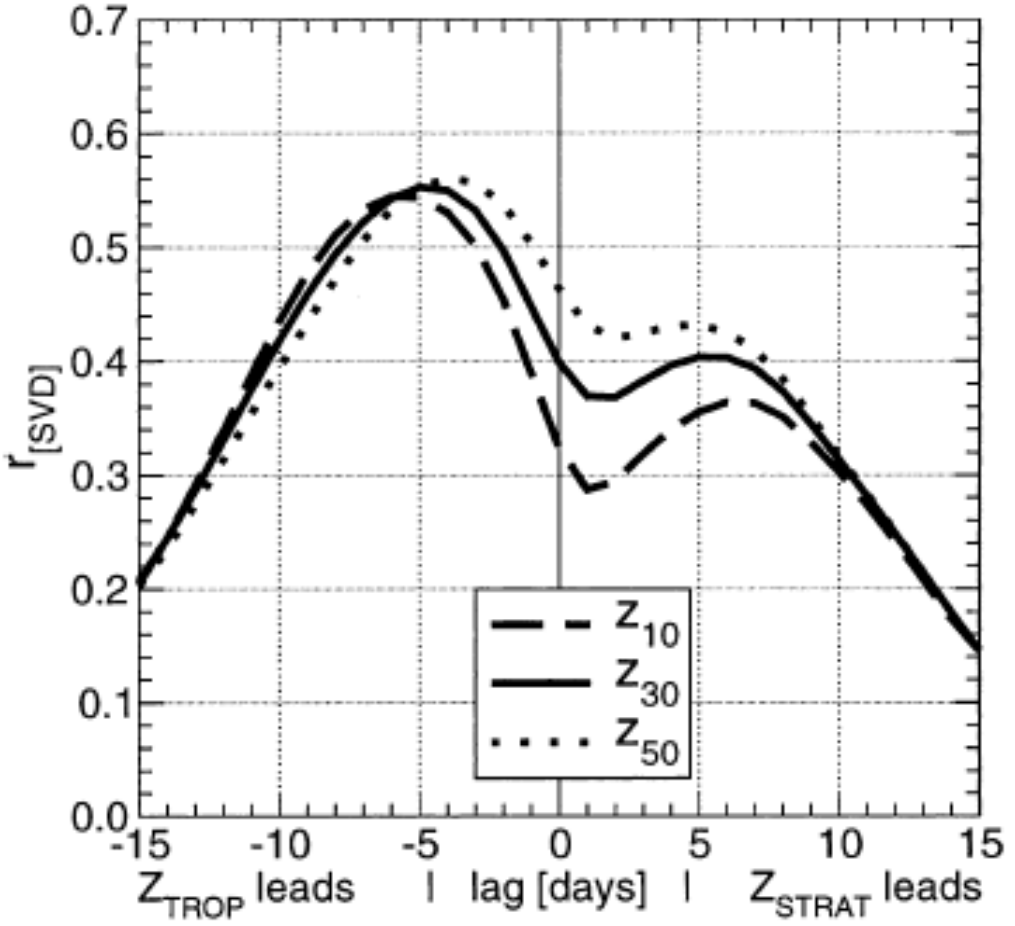

FIG. 2. The r_{SVD}(lag) of the leading coupled mode, which is combined from a series of 31 SVD analyses between the daily time series of Z-ZWN1$_{500}$ and various stratospheric wave 1 fields (Z-ZWN1$_{50}$, Z-ZWN1$_{30}$, and Z-ZWN1$_{10}$) individually for JFM. A positive time lag indicates that the stratospheric field is leading.

Fig. 2 Coarse-grain estimates of Ertel's potential vorticity Q on the 850 K isentropic surface (near the 10-mbar isobaric surface) on 17 (a) and 27 (b) January 1979, at 00 h GMT. The southernmost latitude circle shown is 20° N; the others are 30° N and 60° N. Map projection is polar stereographic. For units see equation (5) onwards. Contour interval is 2 units. Values greater than 4 units are lightly shaded, and greater than 6 units heavily shaded.

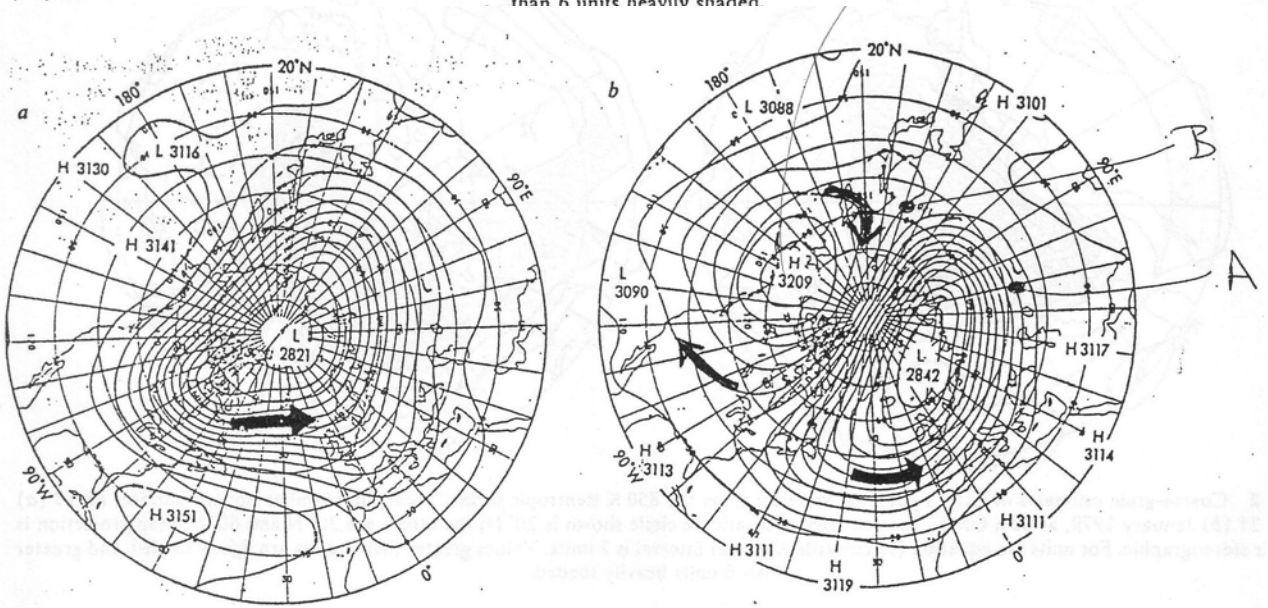

Fig. 1 Geopotential height in decametres (numerically nearly the geometric altitude above sea level) of the 10-mbar isobaric surface on 17 (a) and 27 (b) January 1979, at 00 h GMT. Contour interval is 24 decametres. Map projection is polar stereographic. The southernmost latitude circle shown is 20° N.

That was small breaking. Now for large breaking:

Fig. 2 Coarse-grain estimates of Ertel's potential vorticity Q on the 850 K isentropic surface (near the 10-mbar isobaric surface) on 17 (*a*) and 27 (*b*) January 1979, at 00 h GMT. The southernmost latitude circle shown is 20° N; the others are 30° N and 60° N. Map projection is polar stereographic. For units see equation (5) onwards. Contour interval is 2 units. Values greater than 4 units are lightly shaded, and greater than 6 units heavily shaded.

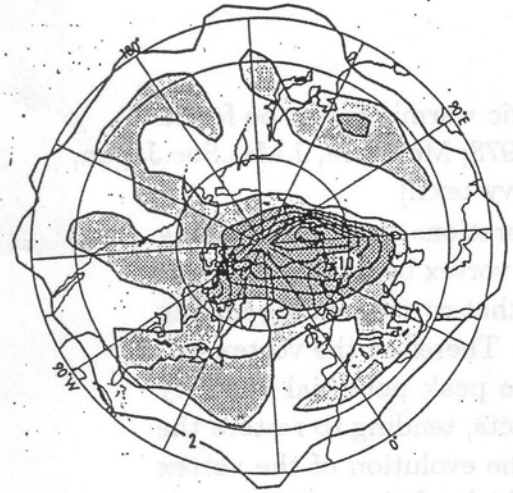

Fig. 4 Ertel's potential vorticity as in Fig. 2, but for 16 February 1979. The shading refers to same contour values as in Fig. 2. The small area of the main vortex suggests that the stratosphere was highly 'preconditioned', that is, susceptible to a major warming.

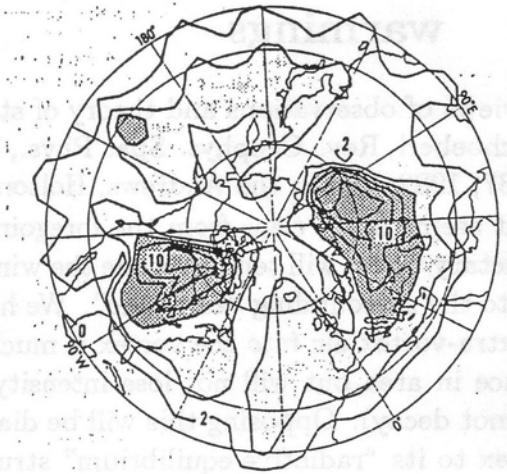

Fig. 5 Ertel's potential vorticity as in Fig. 2, but for 23 February 1979, showing the effect of the subsequent major warming.

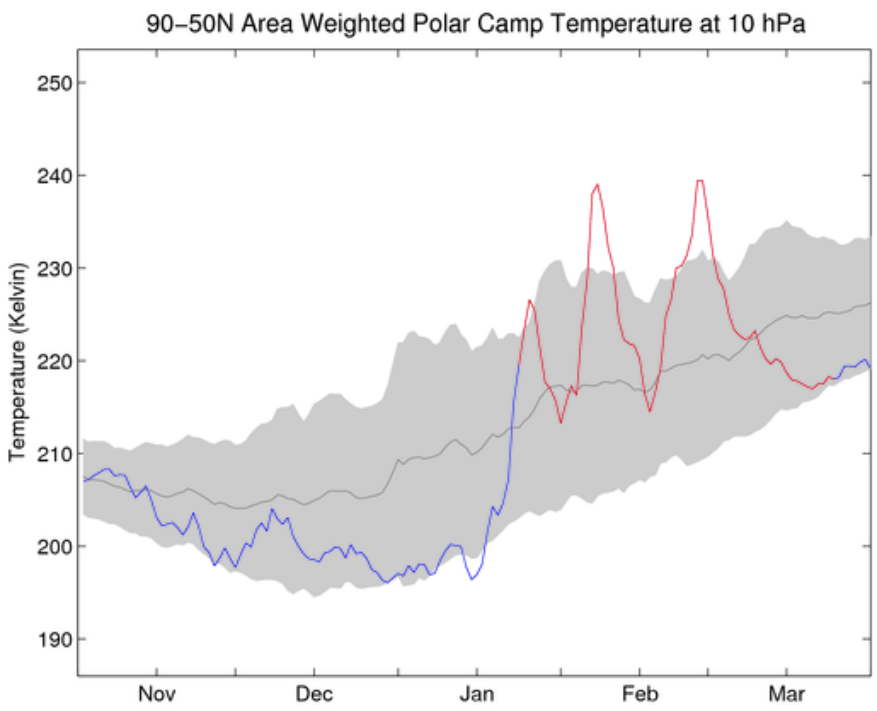
90–50N Area Weighted Polar Camp Temperature at 10 hPa
Temperature (Kelvin)
250
240
230
220
210
200
190
Nov
Dec
Jan
Feb
Mar

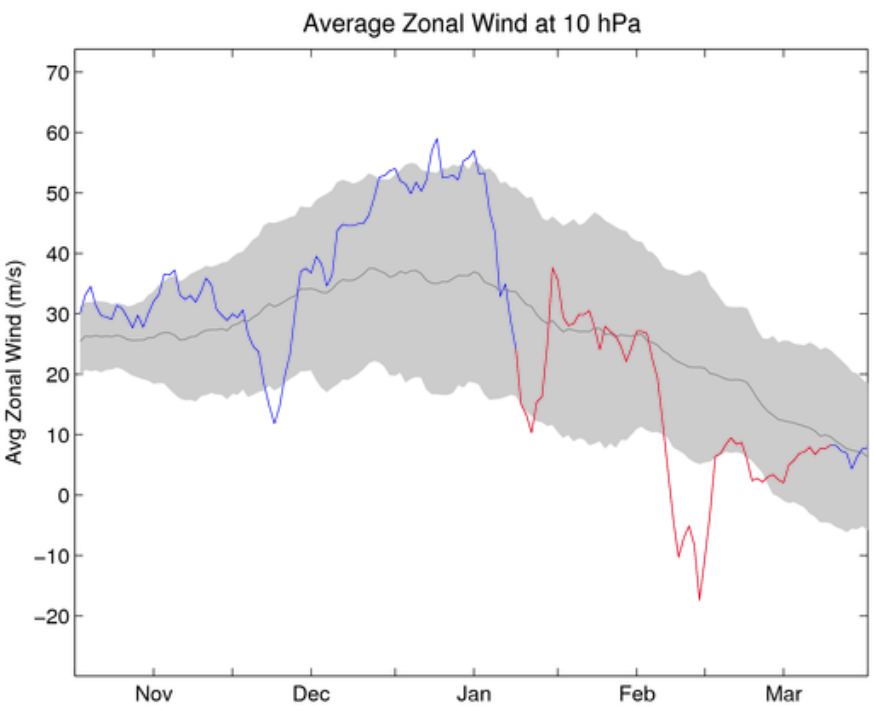
Average Zonal Wind at 10 hPa
Avg Zonal Wind (m/s)
70
60
50
40
30
20
10
0
−10
−20
Nov
Dec
Jan
Feb
Mar

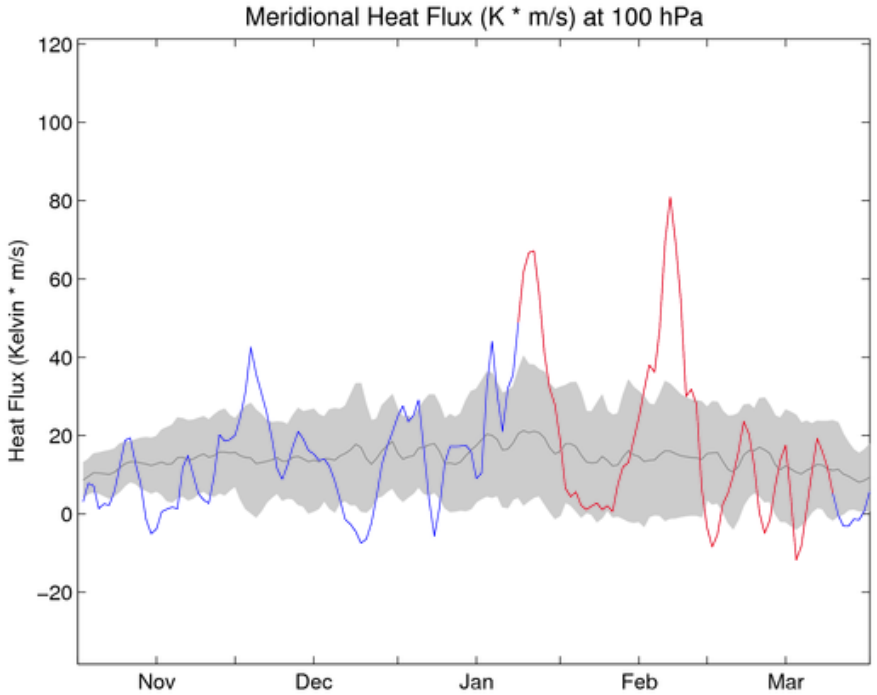
Meridional Heat Flux (K * m/s) at 100 hPa
Heat Flux (Kelvin * m/s)
120
100
80
60
40
20
0
−20
Nov
Dec
Jan
Feb
Mar

22 Feb 1979

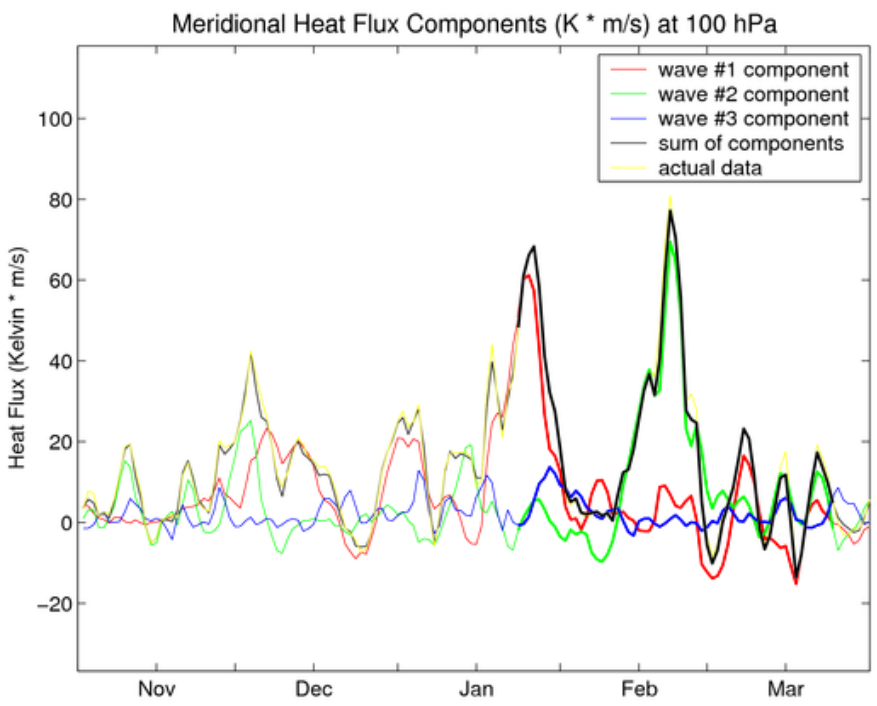
Meridional Heat Flux Components (K * m/s) at 100 hPa
wave #1 component
wave #2 component
wave #3 component
sum of components
actual data
Heat Flux (Kelvin * m/s)
100
80
60
40
20
0
−20
Nov
Dec
Jan
Feb
Mar

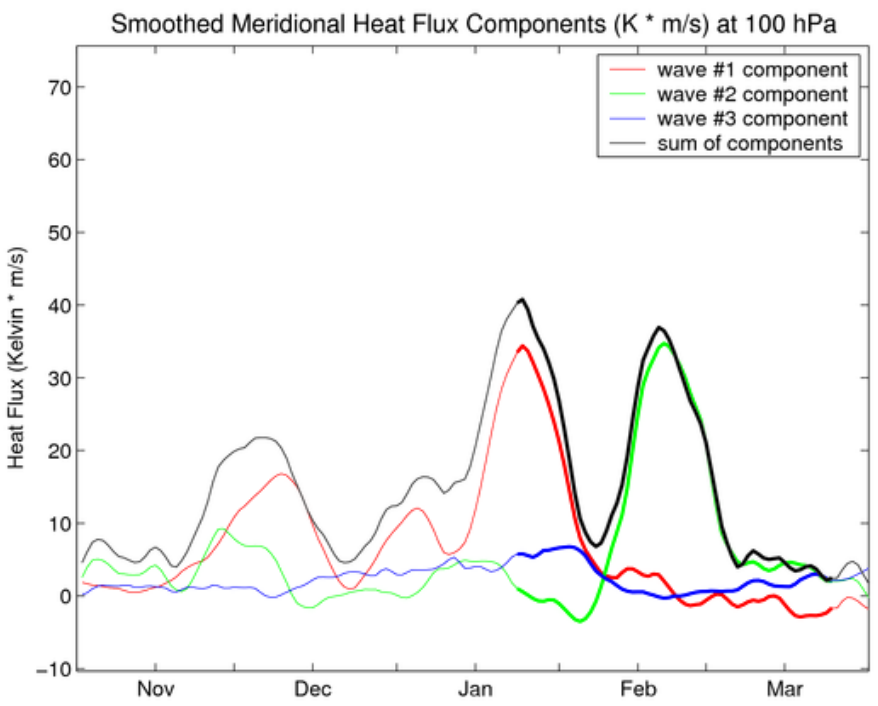
Smoothed Meridional Heat Flux Components (K * m/s) at 100 hPa
wave #1 component
wave #2 component
wave #3 component
sum of components
Heat Flux (Kelvin * m/s)
70
60
50
40
30
20
10
0
−10
Nov
Dec
Jan
Feb
Mar

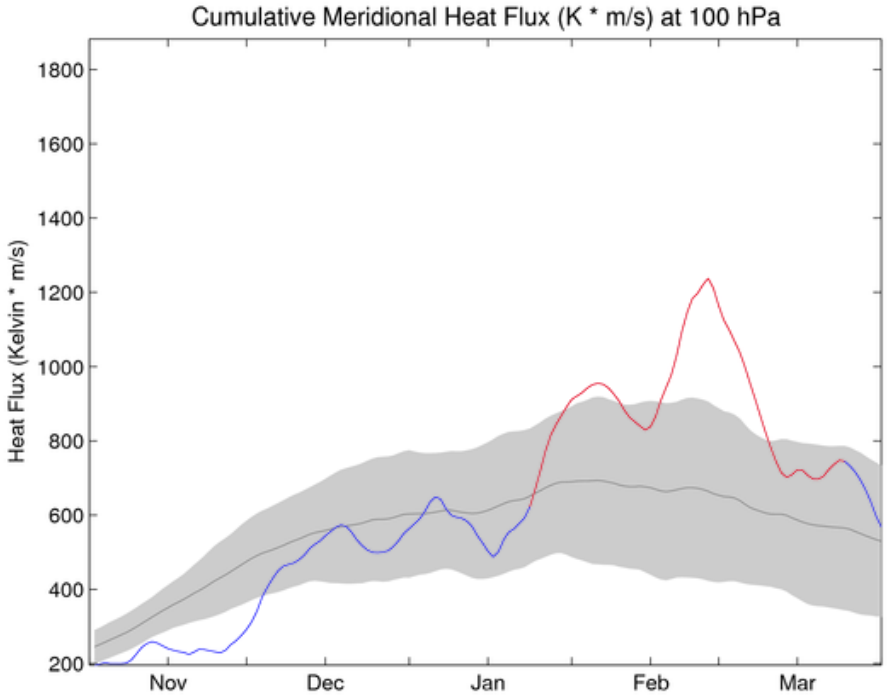
Cumulative Meridional Heat Flux (K * m/s) at 100 hPa
Heat Flux (Kelvin * m/s)
1800
1600
1400
1200
1000
800
600
400
200
Nov
Dec
Jan
Feb
Mar

22 Feb 1979

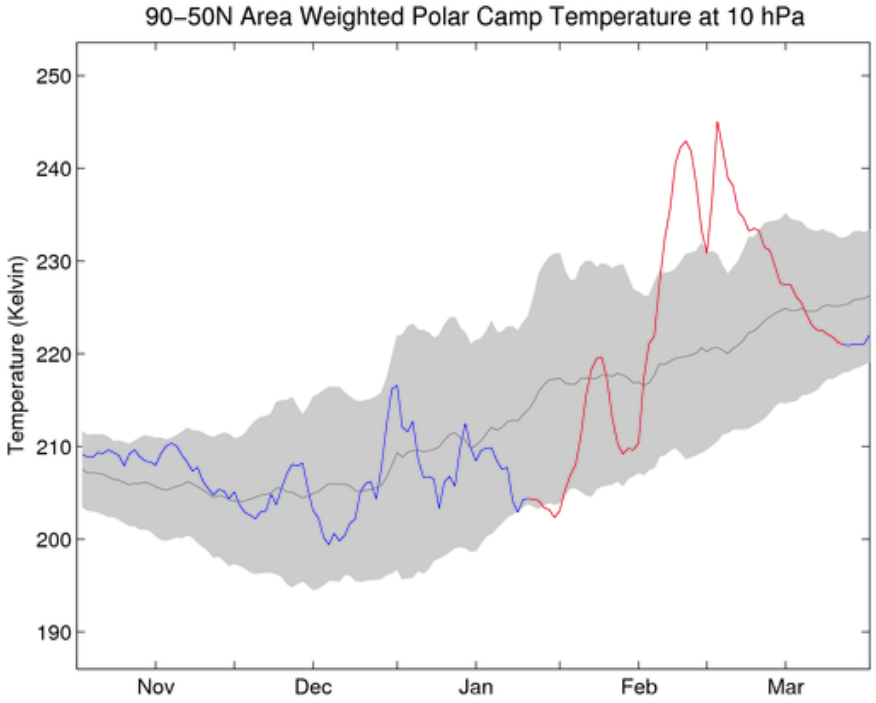
90–50N Area Weighted Polar Camp Temperature at 10 hPa
Temperature (Kelvin)
250
240
230
220
210
200
190
Nov
Dec
Jan
Feb
Mar

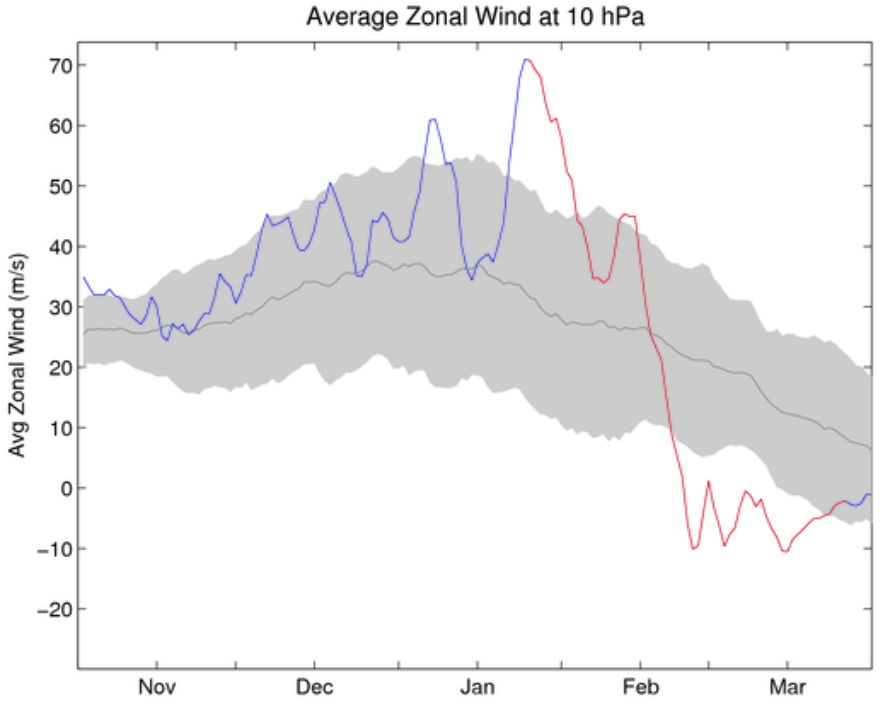
Average Zonal Wind at 10 hPa
Avg Zonal Wind (m/s)
70
60
50
40
30
20
10
0
−10
−20
Nov
Dec
Jan
Feb
Mar

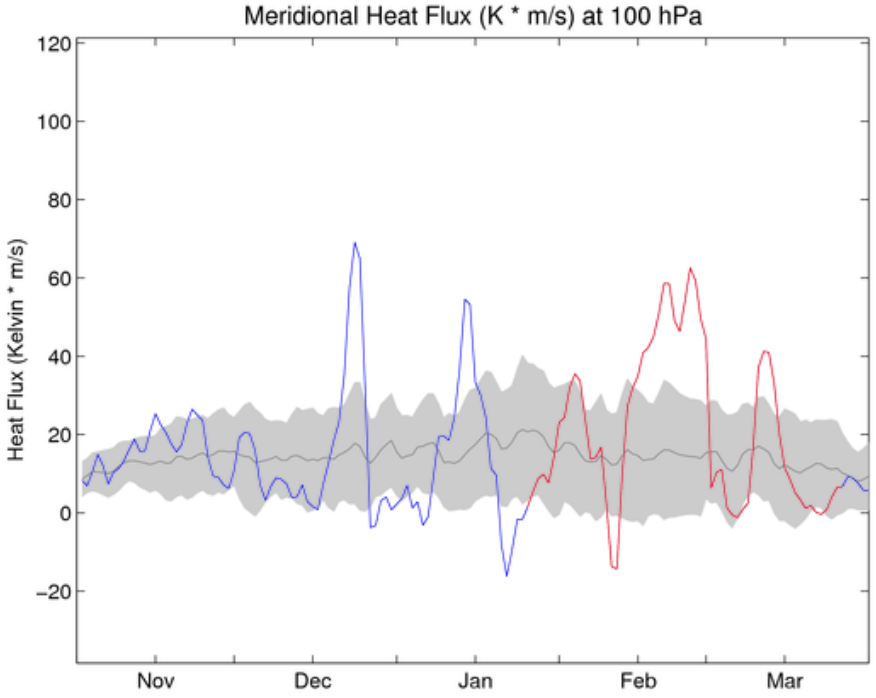
Meridional Heat Flux (K * m/s) at 100 hPa
Heat Flux (Kelvin * m/s)
120
100
80
60
40
20
0
−20
Nov
Dec
Jan
Feb
Mar

24 Feb 1984

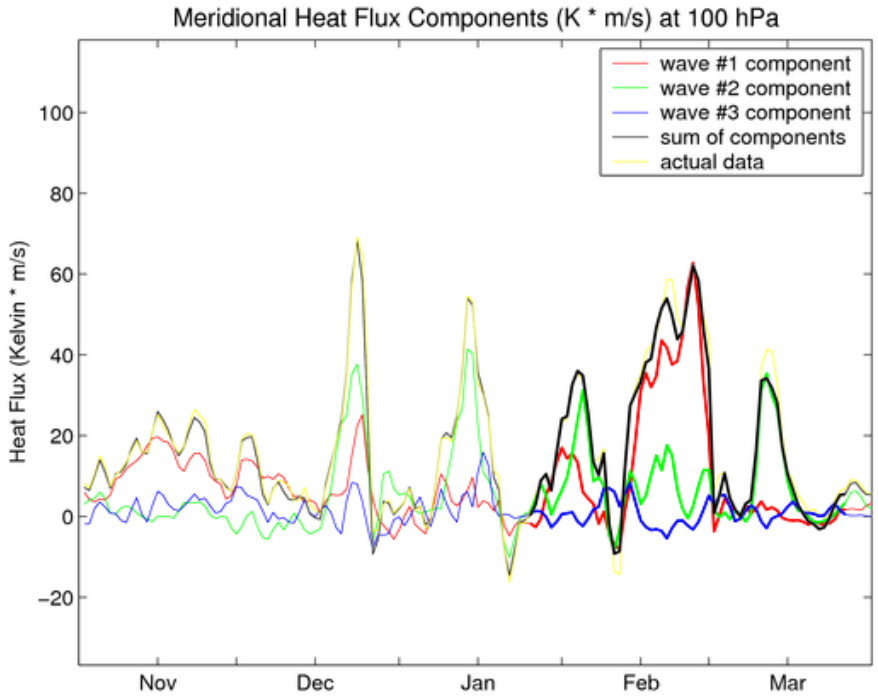
Meridional Heat Flux Components (K * m/s) at 100 hPa
wave #1 component
wave #2 component
wave #3 component
sum of components
actual data
Heat Flux (Kelvin * m/s)
100
80
60
40
20
0
−20
Nov
Dec
Jan
Feb
Mar

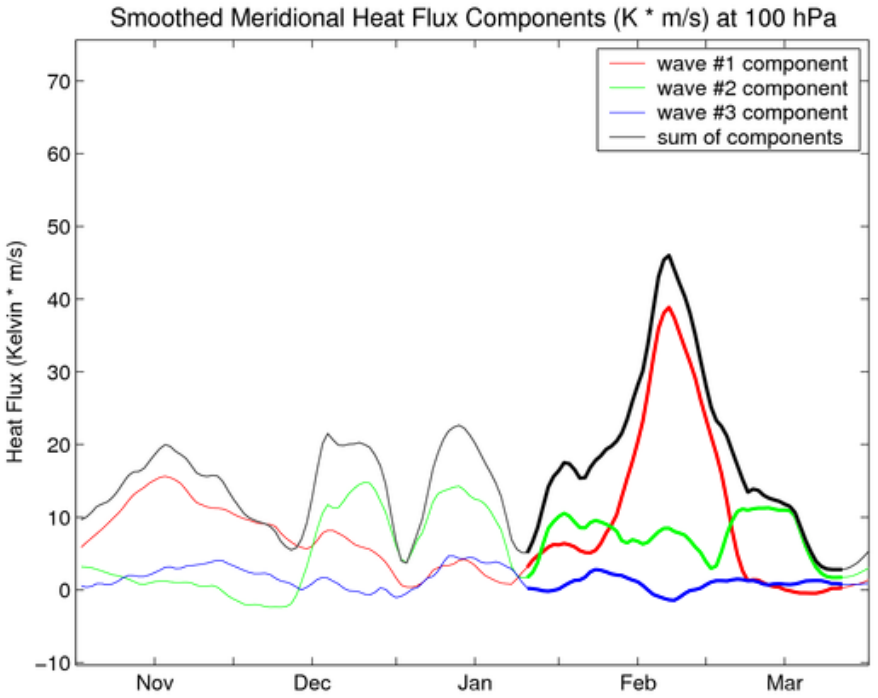
Smoothed Meridional Heat Flux Components (K * m/s) at 100 hPa
wave #1 component
wave #2 component
wave #3 component
sum of components
Heat Flux (Kelvin * m/s)
70
60
50
40
30
20
10
0
−10
Nov
Dec
Jan
Feb
Mar

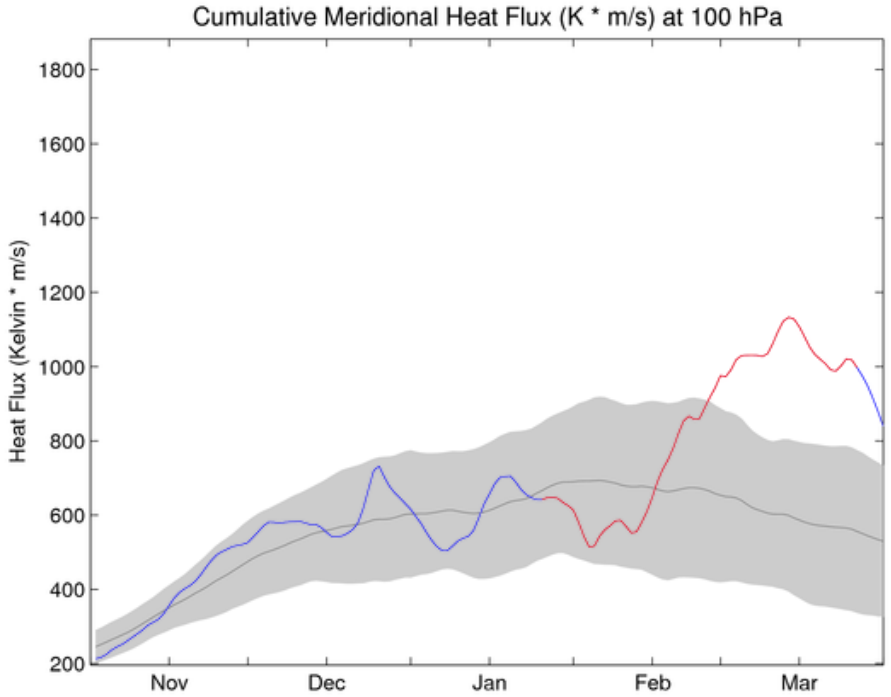
Cumulative Meridional Heat Flux (K * m/s) at 100 hPa
Heat Flux (Kelvin * m/s)
1800
1600
1400
1200
1000
800
600
400
200
Nov
Dec
Jan
Feb
Mar

24 Feb 1984

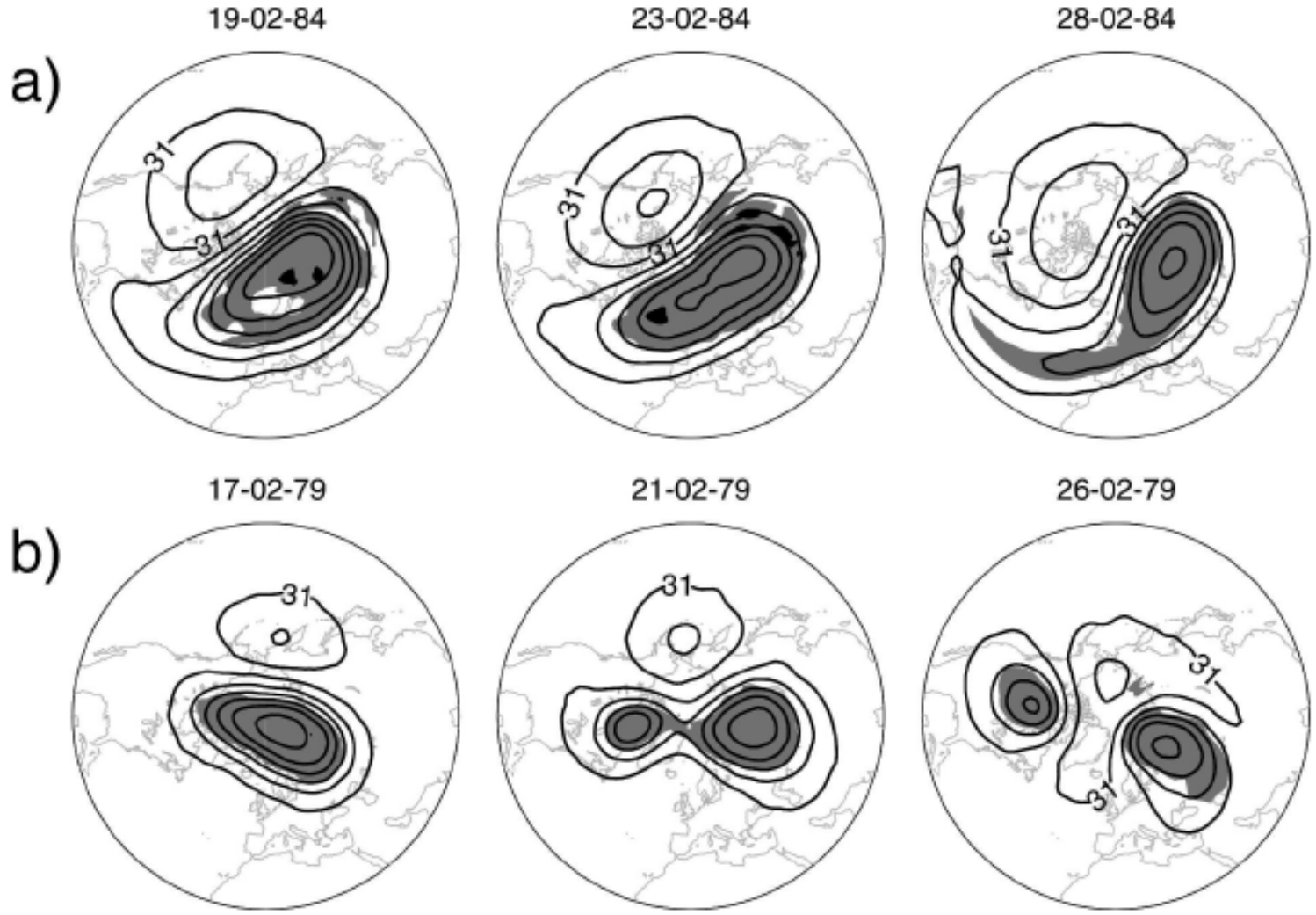

FIG. 1. Polar stereographic plot of geopotential height (contours) on the 10-hPa pressure surface. Contour interval is 0.4 km, and shading shows potential vorticity greater than 4.0×10^{-6} K kg^{-1} m^2 s^{-1}. (a) A vortex displacement type warming that occurred in February 1984. (b) A vortex splitting type warming that occurred in February 1979.

TABLE 1. SSWs identified in NCEP–NCAR and ERA-40 datasets. D indicates a vortex displacement and S indicates a vortex split. ΔT_{10} shows the mean area-weighted polar cap temperature anomaly at 10 hPa ±5 days from the central date. Warmings that are also ESEs [in the sense of Baldwin and Dunkerton (2001), see text] are in bold.

No.	Central date, NCEP–NCAR	Central date, ERA-40	Type subject	Type NCEP–NCAR	Type ERA-40	ΔT_{10} (°K)	References
1	30 Jan 1958	31 Jan 1958	S	S	S	7.8	**Teweles and Finger (1958)**
2	30 Nov 1958		D	D		7.7	**Hare (1960)**
3	16 Jan 1960	15 Jan1960	D	D	D	5.9	
4		28 Jan 1963	S		S	10.5	Finger and Teweles (1964)
5	23 Mar 1965		S	S		4.4	
6	8 Dec 1965	16 Dec 1965	D	D	D	6.7	**Johnson et al. (1969)**
7	24 Feb1966	23 Feb 1966	S	S	S	3.1	Quiroz (1969)
8	8 Jan 1968	7 Jan 1968	S	S	S	12.0	**Johnson et al. (1969)**
9	27 Nov 1968	28 Nov 1968	D	S	D	5.3	
10	13 Mar 1969	13 Mar 1969	D	D	D	4.3	
11	2 Jan 1970	1 Jan 1970	D	D	D	6.8	**Quiroz (1975)**
12	17 Jan 1971	18 Jan 1971	S	S	S	9.6	**Quiroz (1975)**
13	20 Mar 1971	19 Mar 1971	D	D	S	−2.9	
14	2 Feb 1973	31 Jan 1973	S	S	S	6.6	**Quiroz (1975)**
15		9 Jan 1977	S		S	9.1	**O'Neill and Youngblut (1982)**
16	22 Feb 1979	22 Feb 1979	S	S	S	3.7	Palmer (1981)
17	29 Feb 1980	29 Feb 1980	D	D	D	11.5	Baldwin and Holton (1988)
18		4 Mar 1981	D		D	−2.9	
19	4 Dec 1981	4 Dec 1981	D	D	D	0.1	
20	24 Feb 1984	24 Feb 1984	D	D	D	11.1	
21	2 Jan 1985	1 Jan 1985	S	S	S	13.0	Randel and Boville (1987)
22	23 Jan 1987	23 Jan 1987	D	D	D	10.2	**Manney et al. (2005)**
23	8 Dec 1987	7 Dec 1987	S	S	S	14.1	**Baldwin and Dunkerton (1989)**
24	14 Mar 1988	14 Mar 1988	S	D	S	11.7	
25	22 Feb 1989	21 Feb 1989	S	S	S	12.8	**Kruger et al. (2005)**
26	15 Dec 1998	15 Dec 1998	D	D	D	12.7	**Manney et al. (1999)**
27	25 Feb 1999	26 Feb 1999	S	S	S	11.0	**Charlton et al. (2004)**
28	20 Mar 2000	20 Mar 2000	D	D	D	5.3	
29	11 Feb 2001	11 Feb 2001	S	D	D	6.3	**Jacobi et al. (2003)**
30	2 Jan 2002	30 Dec 2001	D	D	D	12.9	Naujokat et al. (2002)
31		17 Feb 2002	D		D	5.6	

Matsuno: dP/Dt>0 → divF<0 → dU/dt<0.

U →0, critical surface forms.
We saw that u'v' goes from postivie to zero atccross the critical srface. Same is tru for v'T' and vertical propagation to critical surface. This implies a step function in F(y), F(z), or a delta function in divF: divF<0.

This also leads to deceleration, which further shifts the critical surface down, casing a downward propagation of U anomalies:

Baldwin and Dunkerton, 2001

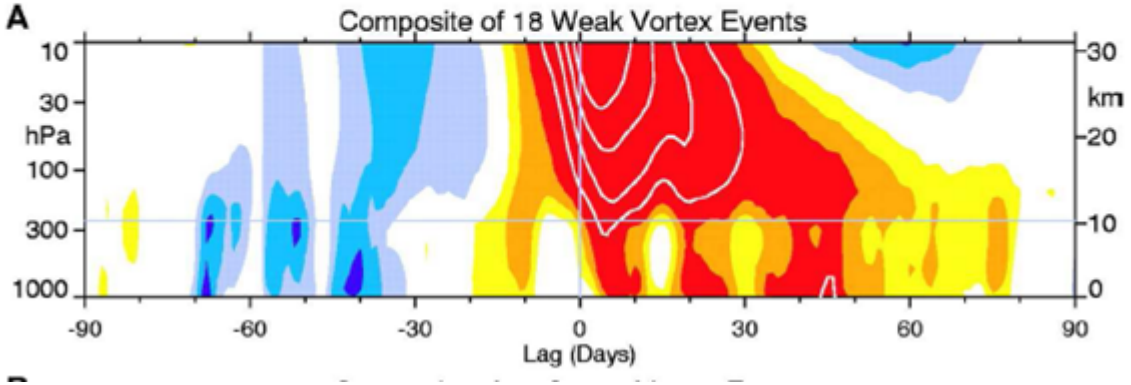

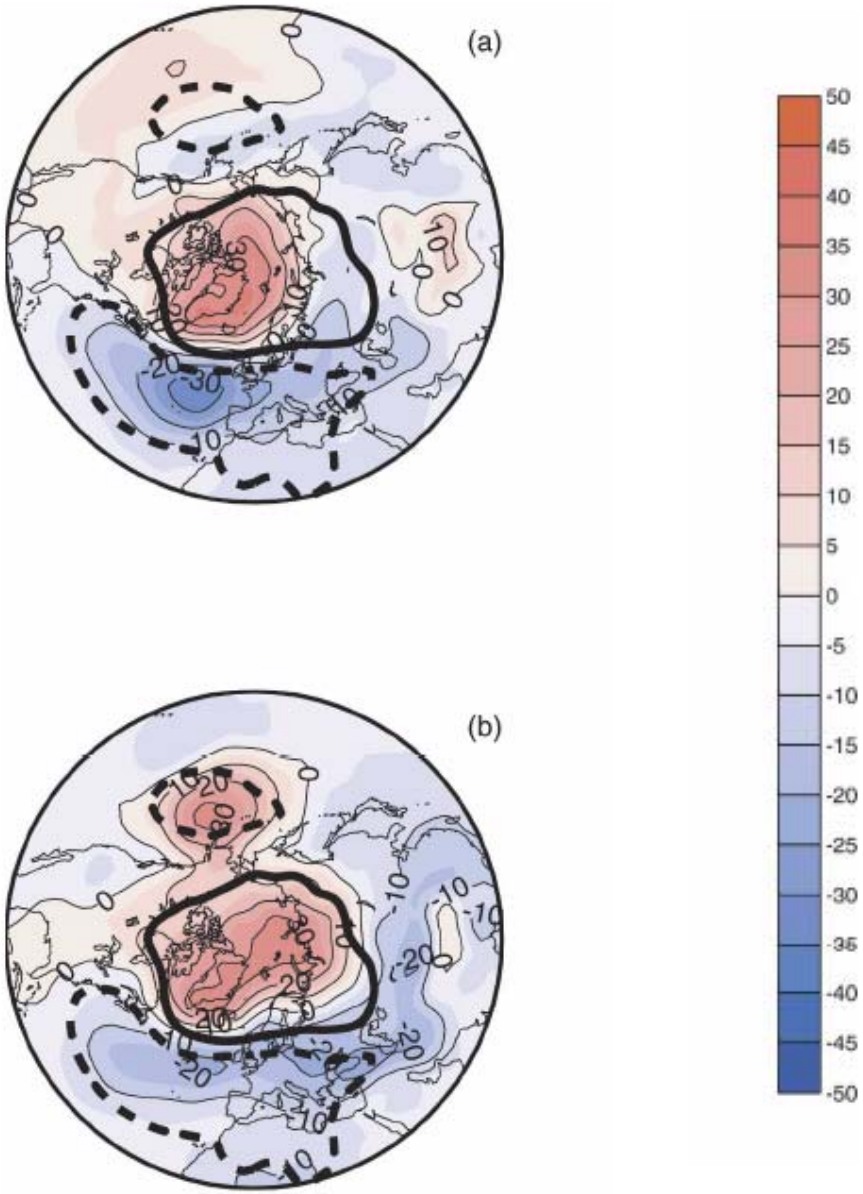

Sudden warmings affect the troposphere

FIG. 10. Mean composite 1000-hPa geopotential height anomalies 0–60 days following different types of stratospheric major warmings. Contour interval is 5 m. Thick black contours show spatial structure of Arctic Oscillation, from data in Baldwin and Dunkerton (2001) (solid and dashed lines show 100 and −100 m values). (a) Composite for all vortex displacements. (b) Same as in (a), but for vortex splits. (c) Difference between vortex displacements and vortex splits; thick black contours denote that difference is significant at 0.1 confidence level. (d) Same as in (a), but only for vortex displacements in Baldwin and Dunkerton (2001). (e) Same as in (d), but

The NH annular mode during stratospheric active season

Thompson and Wallace (2000)

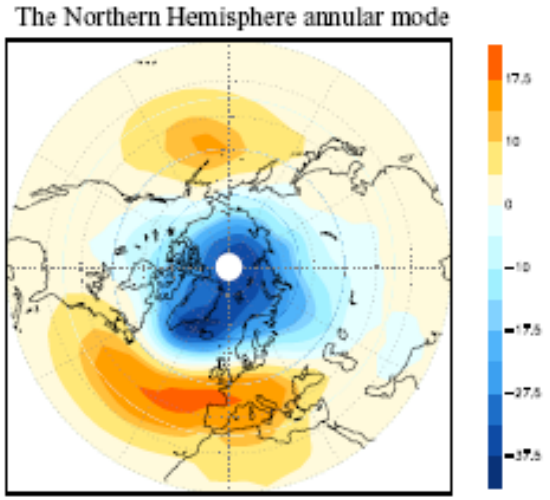

The surface signature of the Northern Hemisphere annular mode. The NAM is defined here as the leading EOF of NH monthly-mean 1000-hPa height anomalies. Units are m/std of the principal component time series.

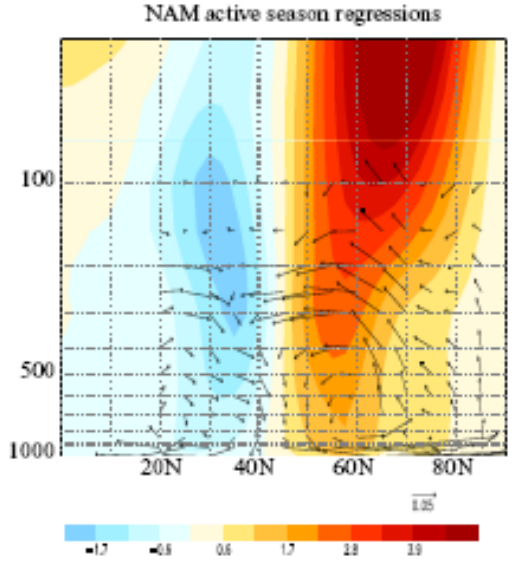

Zonal wind (m/s) and mean meridional circulation anomalies (m/s; cm/s) regressed on January-March values of the NAM index.

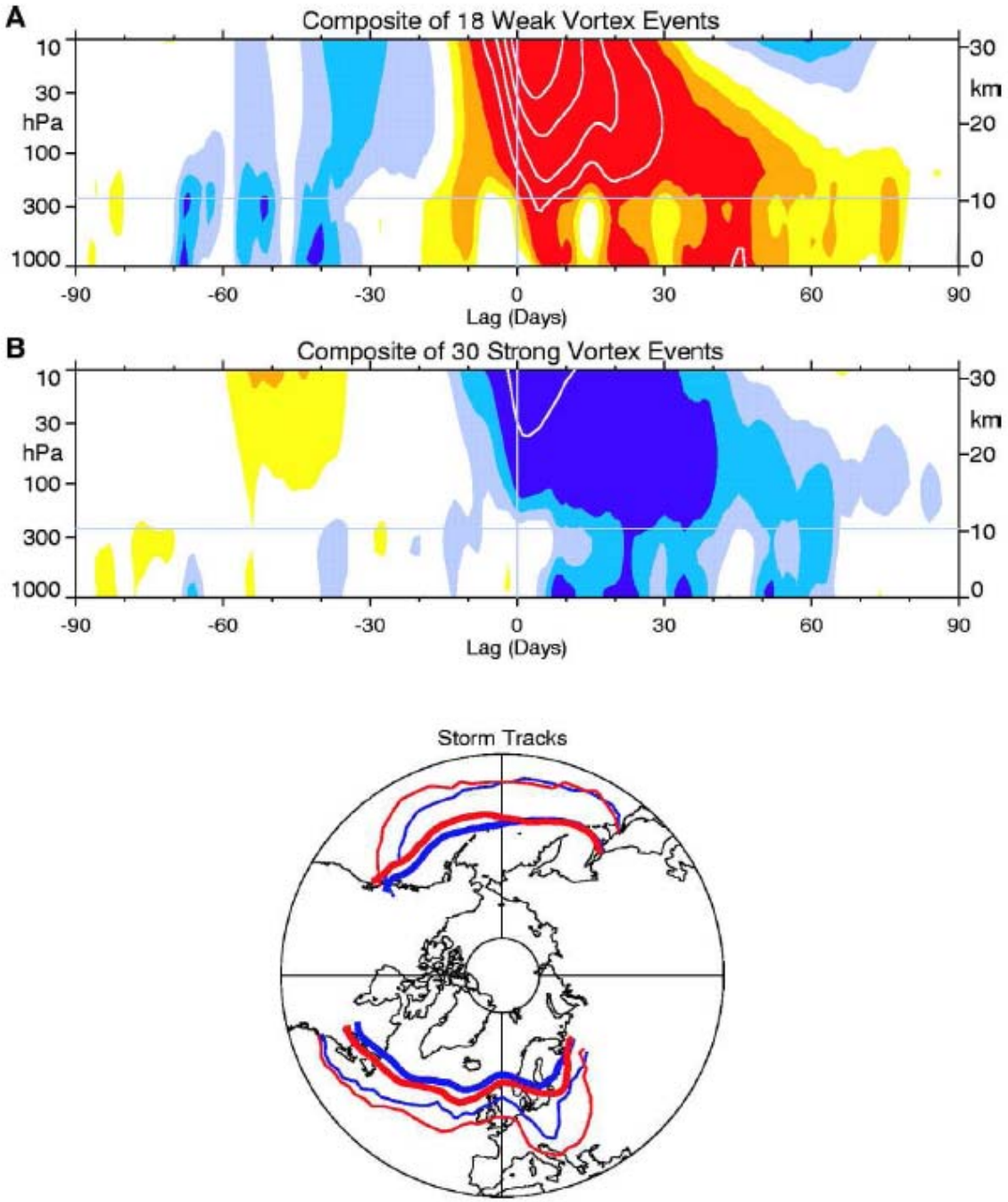
A
Composite of 18 Weak Vortex Events
10
30
hPa
100
300
1000
30
km
20
10
0
-90
-60
-30
0
30
60
90
Lag (Days)
B
Composite of 30 Strong Vortex Events
10
30
hPa
100
300
1000
30
km
20
10
0
-90
-60
-30
0
30
60
90
Lag (Days)
Storm Tracks

Stratospheric Memory and Skill of Extended-Range Weather Forecasts

Mark P. Baldwin,[1] David B. Stephenson,[2] David W. J. Thompson,[3] Timothy J. Dunkerton,[1] Andrew J. Charlton,[2] Alan O'Neill[2]

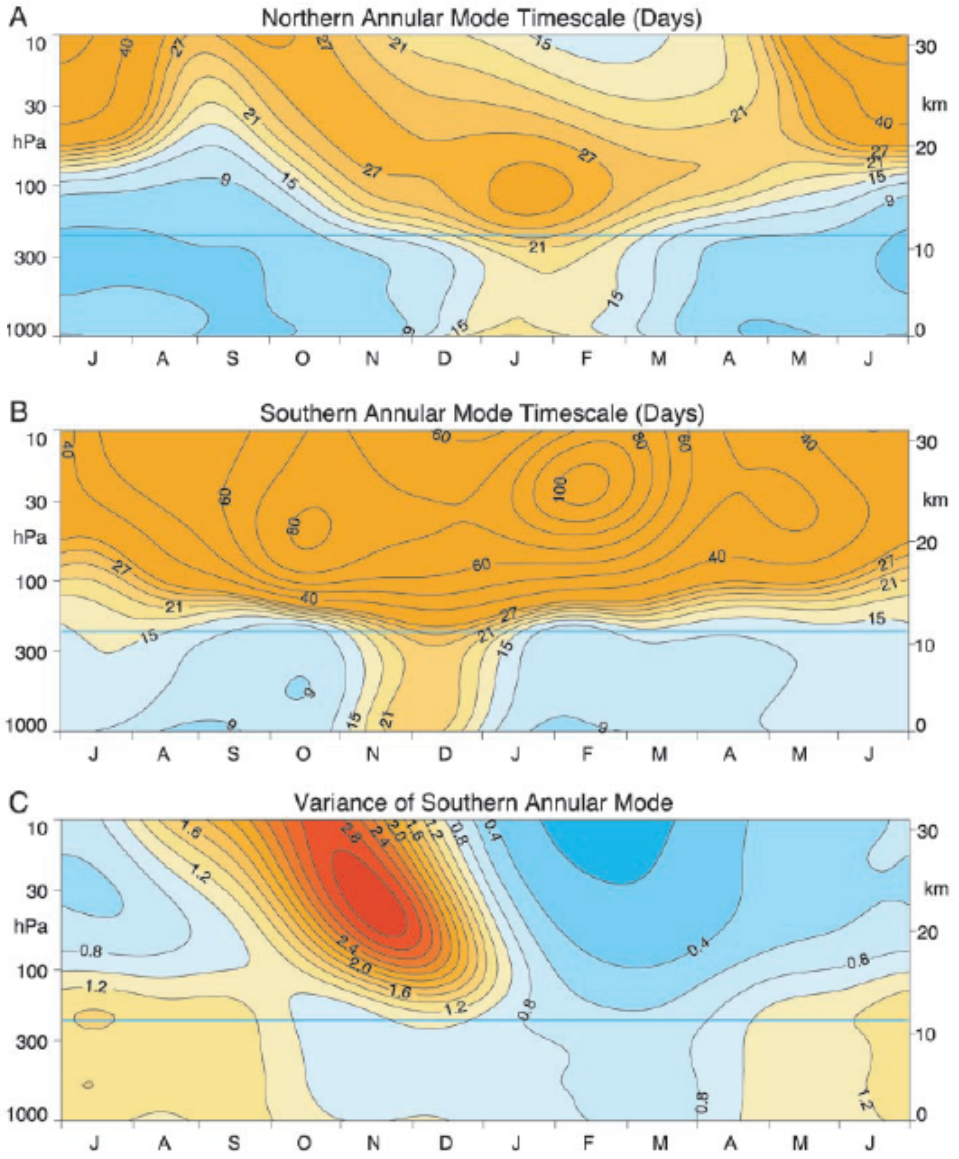

Fig. 1. (**A**) Time scale of the NAM as measured by the time (days) for the autocorrelation function to drop to 1/*e* (~0.378). The horizontal line in each panel represents the approximate tropopause. Daily values are a time average using Gaussian weighting with a full width at half maximum (FWHM) of 60 days (σ = 26 days). The time scale is estimated with a least-squares fit of an exponential curve to the autocorrelation function. The contour interval is 3 days up to 30 days, and 10 days at higher values. (**B**) The time scale of the SAM, measured as in (A). (**C**) Variance of the SAM. Daily values were obtained with the same methodology as in (A). The SAM time series at each level are normalized to unit standard deviation.

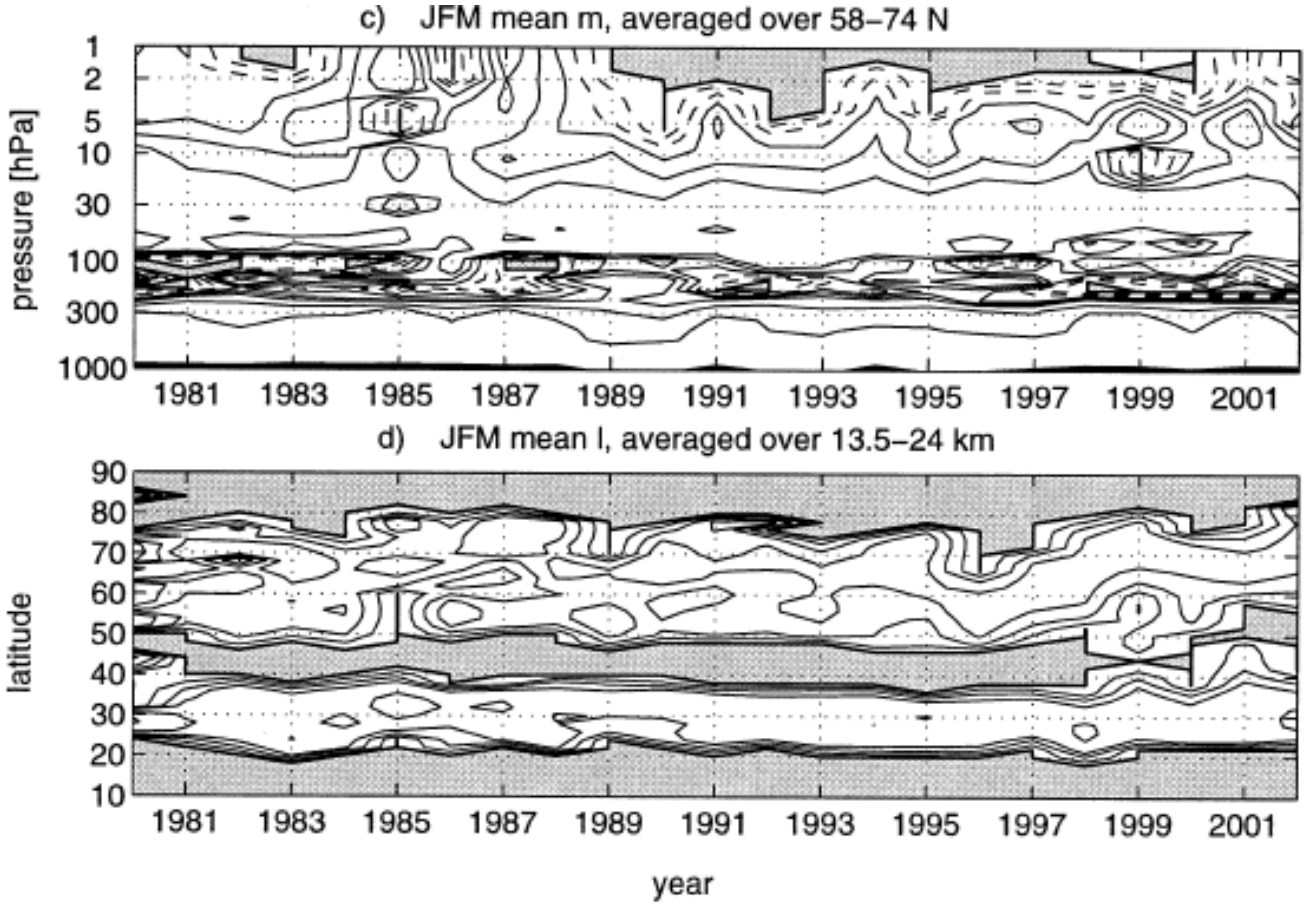

FIG. 8. (a) The vertical wavenumbers, calculated from the SON mean basic states for the years 1979–2001, averaged over 58°–74°N. (b) The meridional wavenumbers, calculated from the SON mean basic states for the years 1979–2001, averaged over 13.5–24 km. (c),(d) Same as (a),(b), respectively, but for JFM 1980–2002. Vertical wavenumber contours (units of 10^{-5} m^{-1}) are shown at 0.01 (thick line); 2, 4 (dashed); and 6, 8, 10, 15, 20 (solid). Meridional wavenumber contour interval is 1 rad^{-1}, and the 0.01 line is thick.

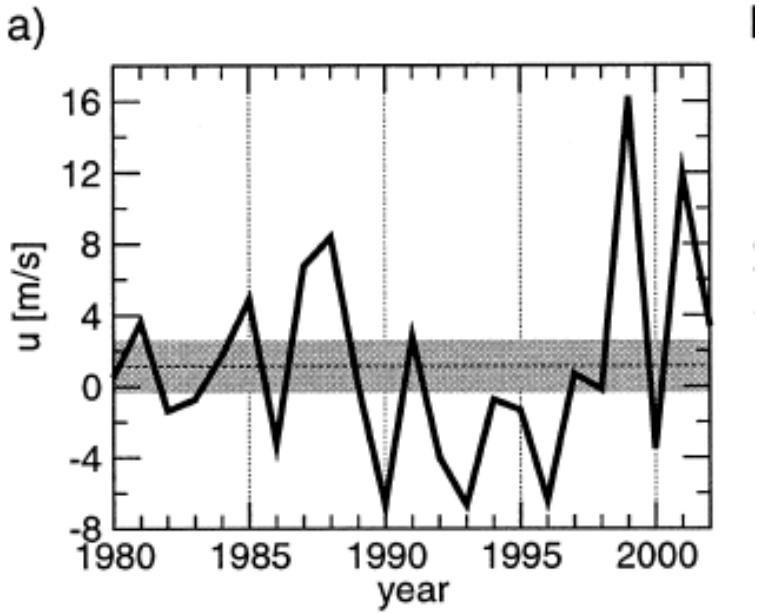

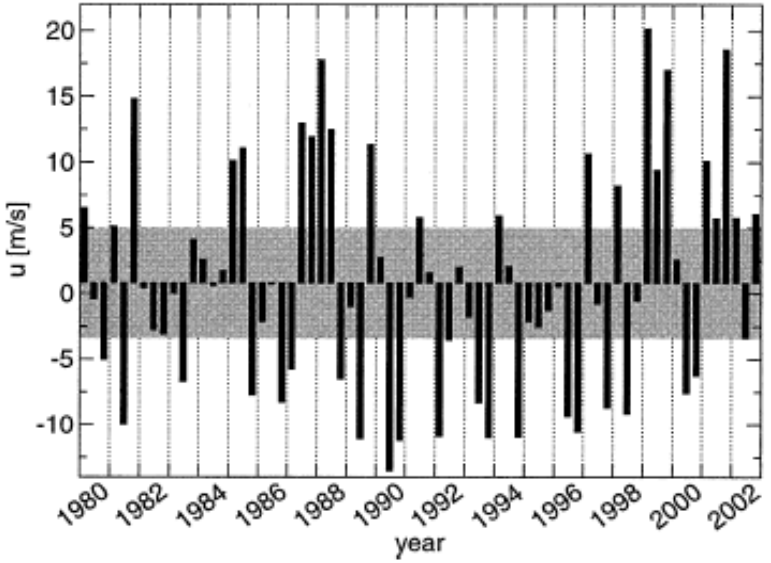

FIG. 10. The time series of monthly mean $U(2–10)$ of JFM. The shading indicates the region of the long-term average ± 0.5 std devs.

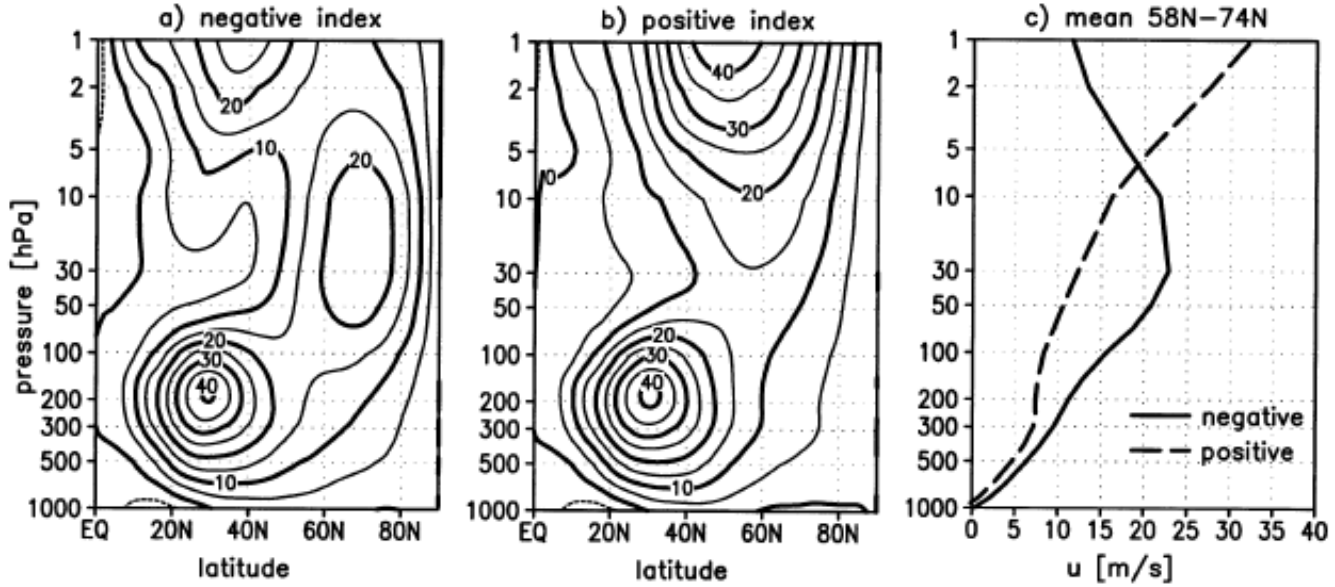

FIG. 11. Composites of monthly mean zonal-mean winds $\overline{u}$ (m s^{-1}) for the (a) negative and (b) positive index $U(2–10)$, based on 0.5 std dev. (c) Composites of vertical profile of $\overline{u}$ (m s^{-1}) averaged between 58° and 74°N.

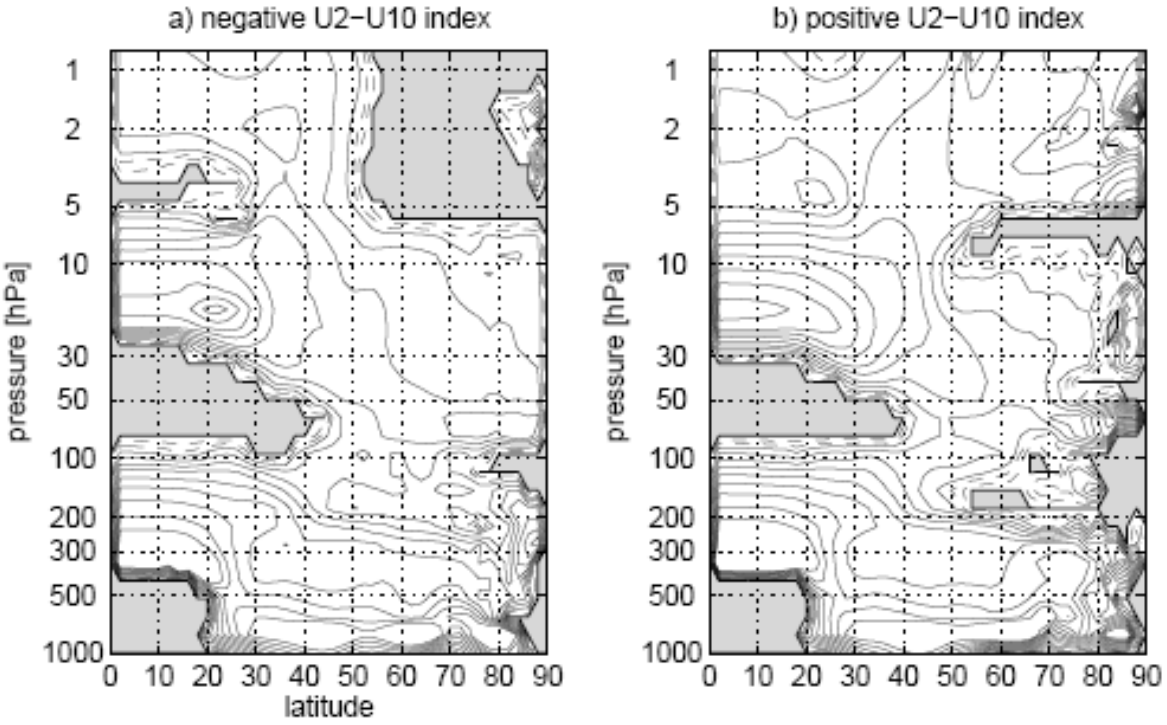
a) negative U2−U10 index
b) positive U2−U10 index
pressure [hPa]
1
2
5
10
30
50
100
200
300
500
1000
0 10 20 30 40 50 60 70 80 90
latitude

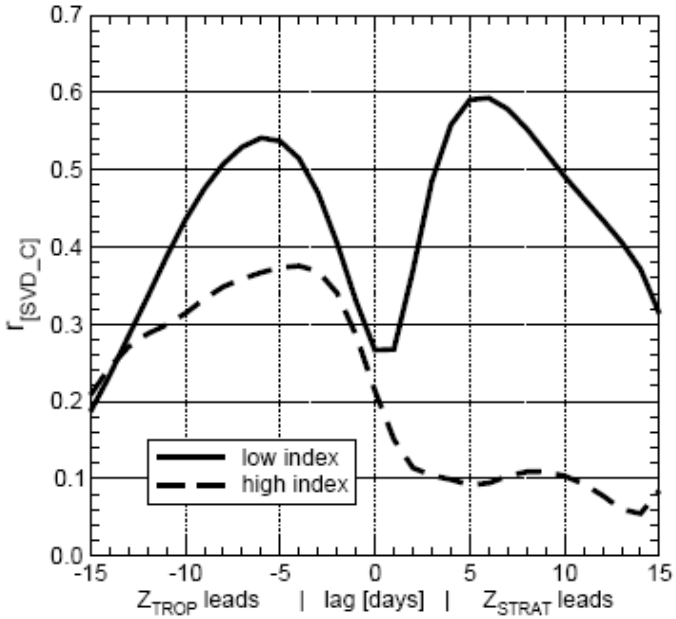
r[SVD_C]
0.0
0.1
0.2
0.3
0.4
0.5
0.6
0.7
low index
high index
-15 -10 -5 0 5 10 15
ZTROP leads | lag [days] | ZSTRAT leads

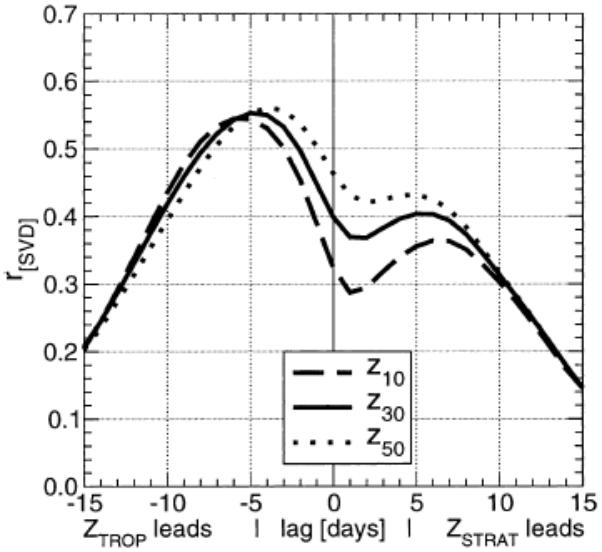

FIG. 2. The r_{SVD}(lag) of the leading coupled mode, which is combined from a series of 31 SVD analyses between the daily time series of Z-ZWN1$_{500}$ and various stratospheric wave 1 fields (Z-ZWN1$_{50}$, Z-ZWN1$_{30}$, and Z-ZWN1$_{10}$) individually for JFM. A positive time lag indicates that the stratospheric field is leading.

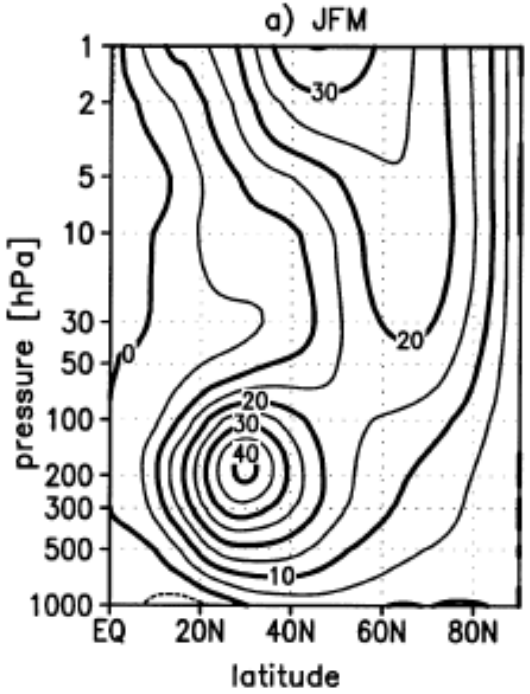

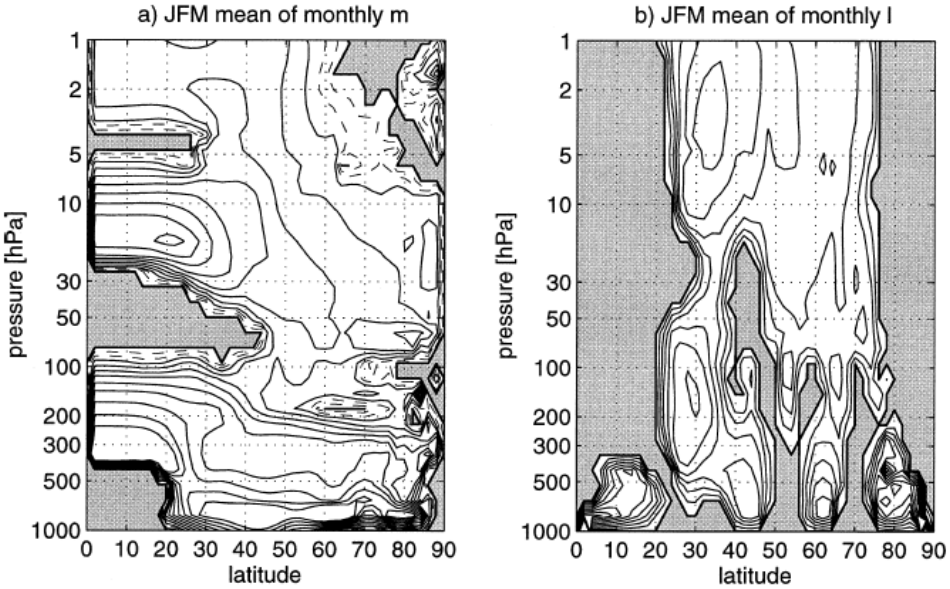

FIG. 4. The (a) vertical and (b) meridional wavenumbers, calculated by averaging the wavenumbers for the monthly mean basic states for each of the JFM months during these years. Vertical wavenumber contours (units of 10^{-5} m^{-1}) are shown at 0.01 (thick line); 2, 4 (dashed); and 6–30 in jumps of 3 (solid). Meridional wavenumber contour interval is 1 rad^{-1}, and the 0.01 line is thick.

TABLE 1. SSWs identified in NCEP–NCAR and ERA-40 datasets. D indicates a vortex displacement an
ΔT_{10} shows the mean area-weighted polar cap temperature anomaly at 10 hPa ±5 days from the central da
ESEs [in the sense of Baldwin and Dunkerton (2001), see text] are in bold.

No.	Central date, NCEP–NCAR	Central date, ERA-40	Type subject	Type NCEP–NCAR	Type ERA-40	ΔT_{10} (°K)	
1	30 Jan 1958	31 Jan 1958	S	S	S	7.8	**Tew**
2	30 Nov 1958		D	D		7.7	**Hare**
3	16 Jan 1960	15 Jan1960	D	D	D	5.9	
4		28 Jan 1963	S		S	10.5	Fing
5	23 Mar 1965		S	S		4.4	
6	8 Dec 1965	16 Dec 1965	D	D	D	6.7	**John**
7	24 Feb1966	23 Feb 1966	S	S	S	3.1	Quir
8	8 Jan 1968	7 Jan 1968	S	S	S	12.0	**Johnson et al. (1969)**
9	27 Nov 1968	28 Nov 1968	D	S	D	5.3	
10	13 Mar 1969	13 Mar 1969	D	D	D	4.3	
11	2 Jan 1970	1 Jan 1970	D	D	D	6.8	**Quiroz (1975)**
12	17 Jan 1971	18 Jan 1971	S	S	S	9.6	**Quiroz (1975)**
13	20 Mar 1971	19 Mar 1971	D	D	S	−2.9	
14	2 Feb 1973	31 Jan 1973	S	S	S	6.6	**Quiroz (1975)**
15		9 Jan 1977	S		S	9.1	**O'Neill and Youngblut (1982)**
16	22 Feb 1979	22 Feb 1979	S	S	S	3.7	Palmer (1981)
17	29 Feb 1980	29 Feb 1980	D	D	D	11.5	Baldwin and Holton (1988)
18		4 Mar 1981	D		D	−2.9	
19	4 Dec 1981	4 Dec 1981	D	D	D	0.1	
20	24 Feb 1984	24 Feb 1984	D	D	D	11.1	
21	2 Jan 1985	1 Jan 1985	S	S	S	13.0	Randel and Boville (1987)
22	23 Jan 1987	23 Jan 1987	D	D	D	10.2	**Manney et al. (2005)**
23	8 Dec 1987	7 Dec 1987	S	S	S	14.1	**Baldwin and Dunkerton (1989)**
24	14 Mar 1988	14 Mar 1988	S	D	S	11.7	
25	22 Feb 1989	21 Feb 1989	S	S	S	12.8	**Kruger et al. (2005)**
26	15 Dec 1998	15 Dec 1998	D	D	D	12.7	**Manney et al. (1999)**
27	25 Feb 1999	26 Feb 1999	S	S	S	11.0	**Charlton et al. (2004)**
28	20 Mar 2000	20 Mar 2000	D	D	D	5.3	
29	11 Feb 2001	11 Feb 2001	S	D	D	6.3	**Jacobi et al. (2003)**
30	2 Jan 2002	30 Dec 2001	D	D	D	12.9	Naujokat et al. (2002)
31		17 Feb 2002	D		D	5.6	

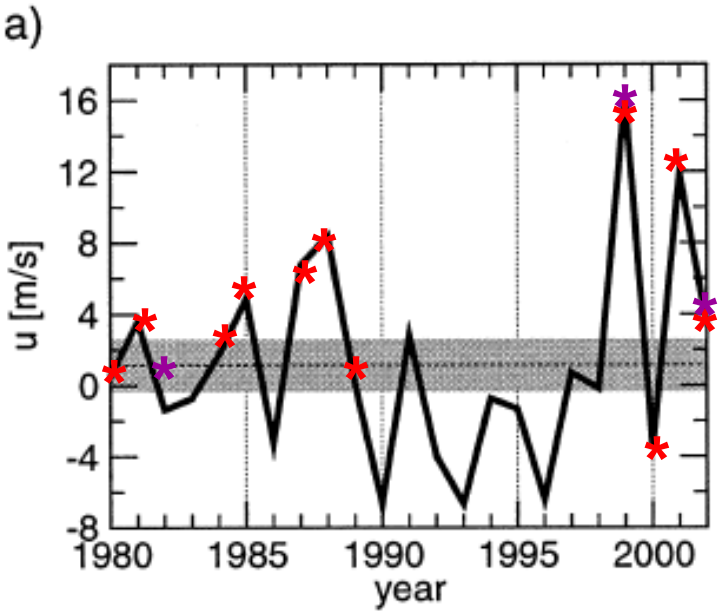

* JFM

* Dec

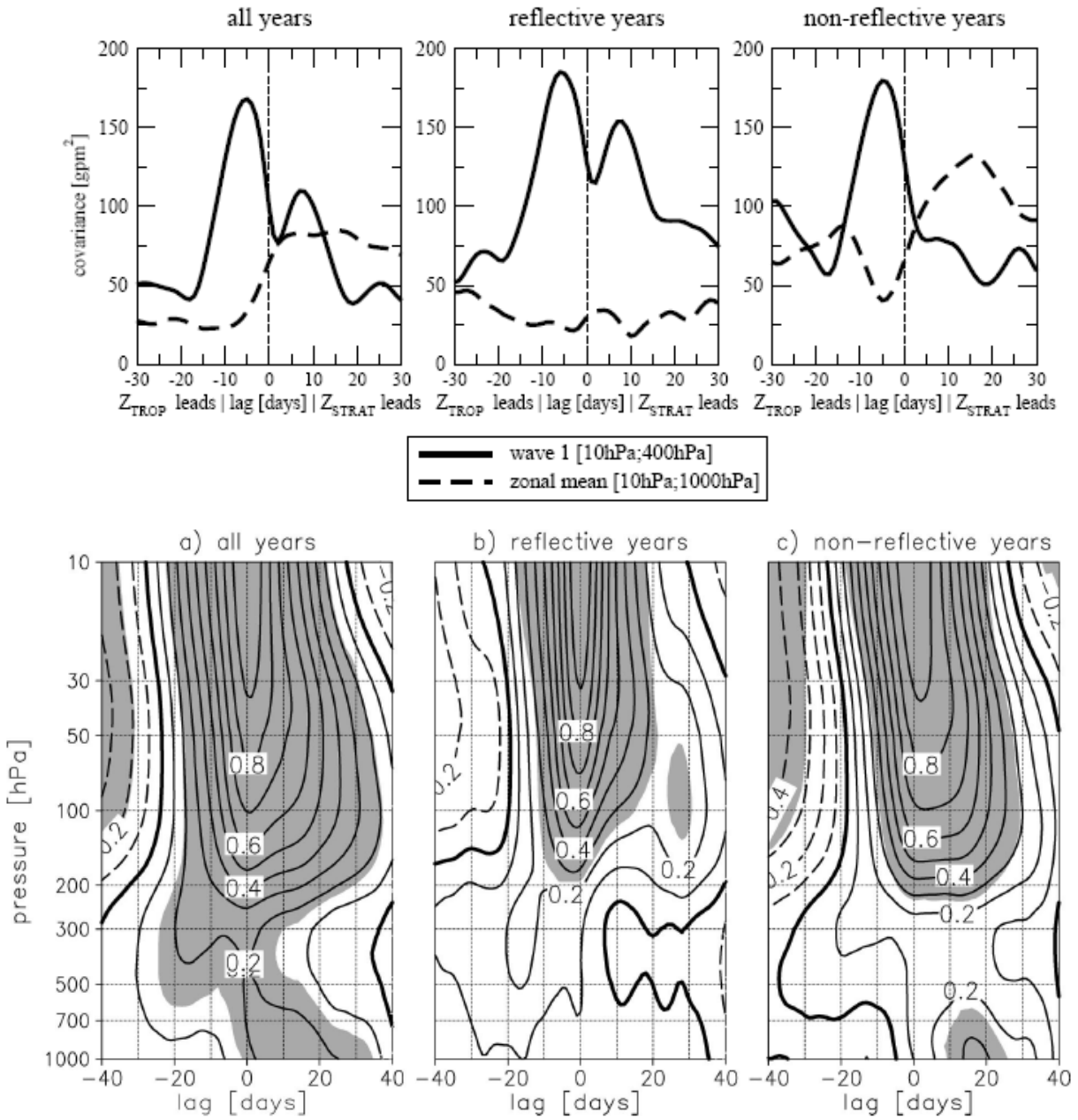

FIG. 4. Correlation coefficients between the NAM signature time series at 10 hPa and at the levels between 1000 and 10 hPa for time lags between −40 and 40 days for (a) all winters 1980–2003, (b) reflective years, and (c) nonreflective years. The thick line represents a value of 0; negative values are dashed. The shading indicates where the correlations coefficients are significant at least at the 95% level taking into account the autocorrelation in the time series. A positive time lag indicates that the 10-hPa time series is leading.

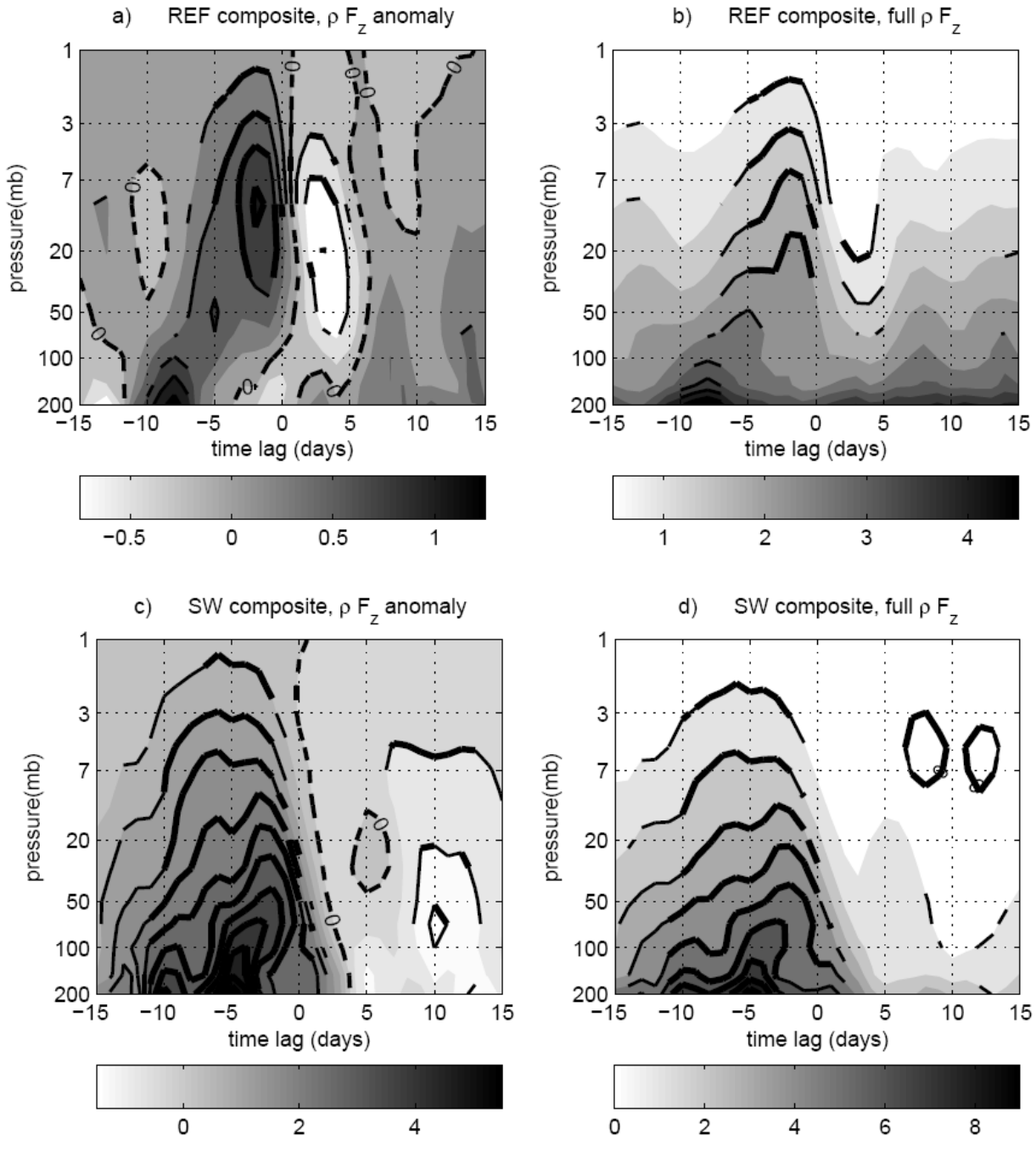
a) REF composite, ρ F_z anomaly
b) REF composite, full ρ F_z
c) SW composite, ρ F_z anomaly
d) SW composite, full ρ F_z
pressure(mb)
time lag (days)
1
3
7
20
50
100
200
−15
−10
−5
0
5
10
15
−0.5
0
0.5
1
2
3
4
6
8

Arctic vs Antarctic

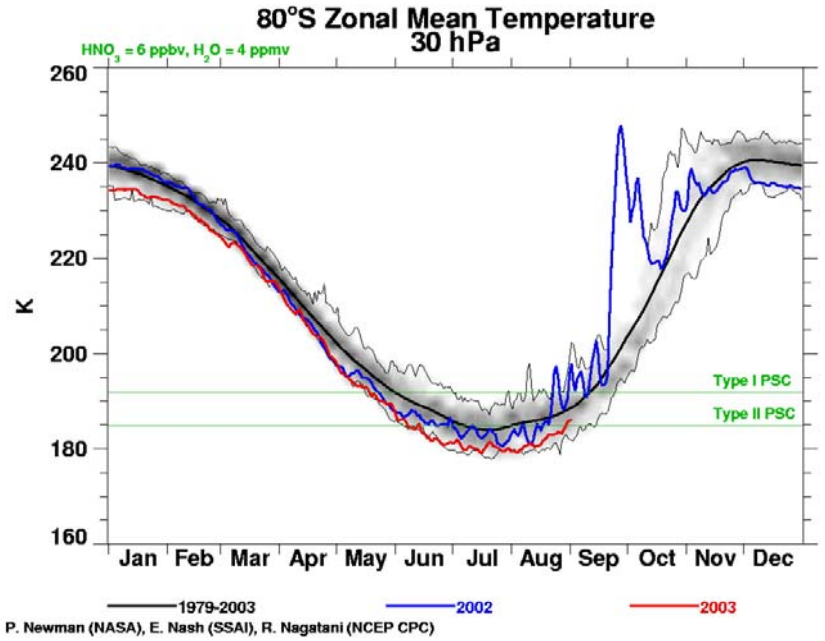

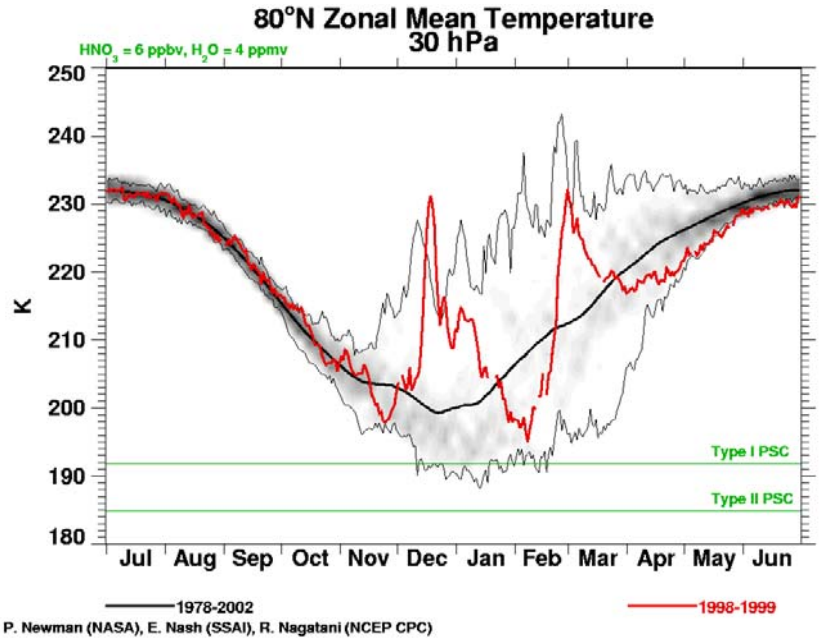

Year to year changes

Second Largest Ozone Hole Area

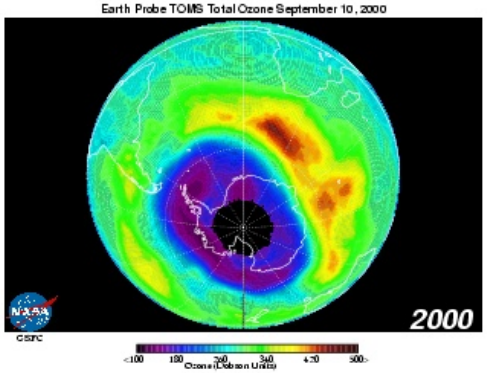

Maximum Area = 11.5 million square miles

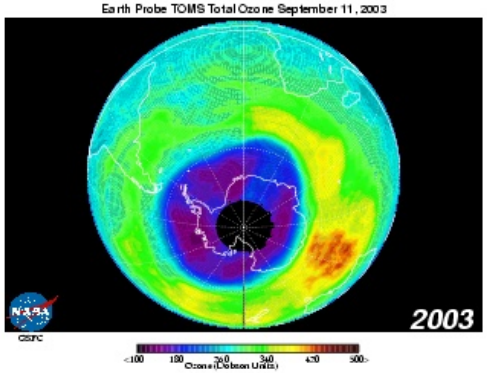

Maximum Area = 10.9 million square miles

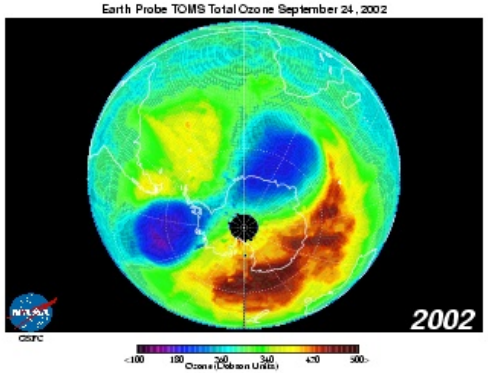

Maximum Area = 8.1 million square miles

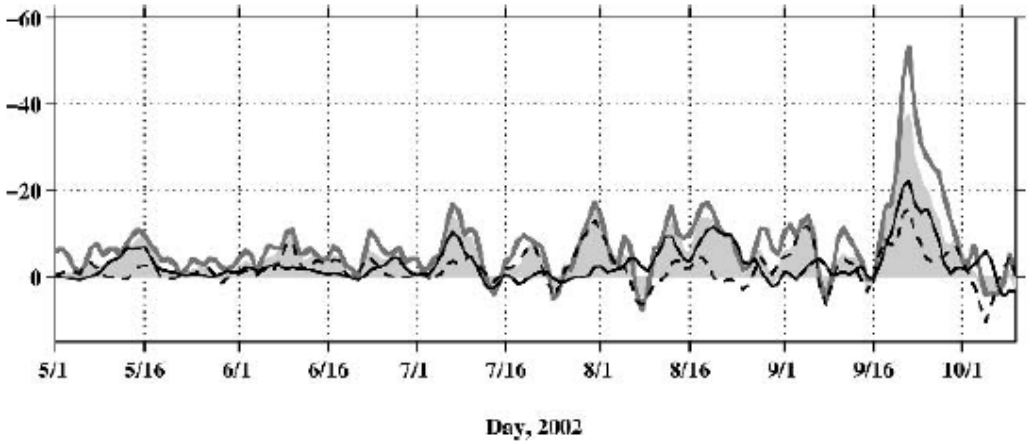

FIG. 1. The 1 May–10 Oct 2002 daily time series of 100-hPa heat fluxes (averaged over 30°–90°S), for wave 1 (solid black), wave 2 (dashed), total (thick gray line), and the sum of waves 1 and 2 (shaded). Units are K m s^{-1}. Note that the vertical axis is flipped, with negative values (upward wave flux) up.

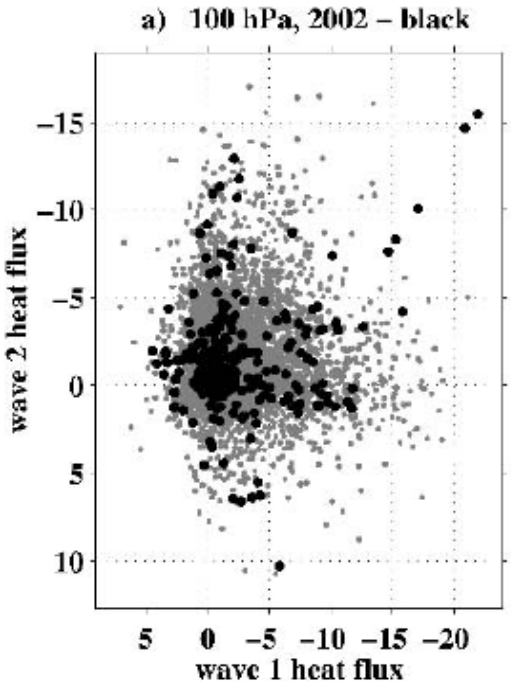

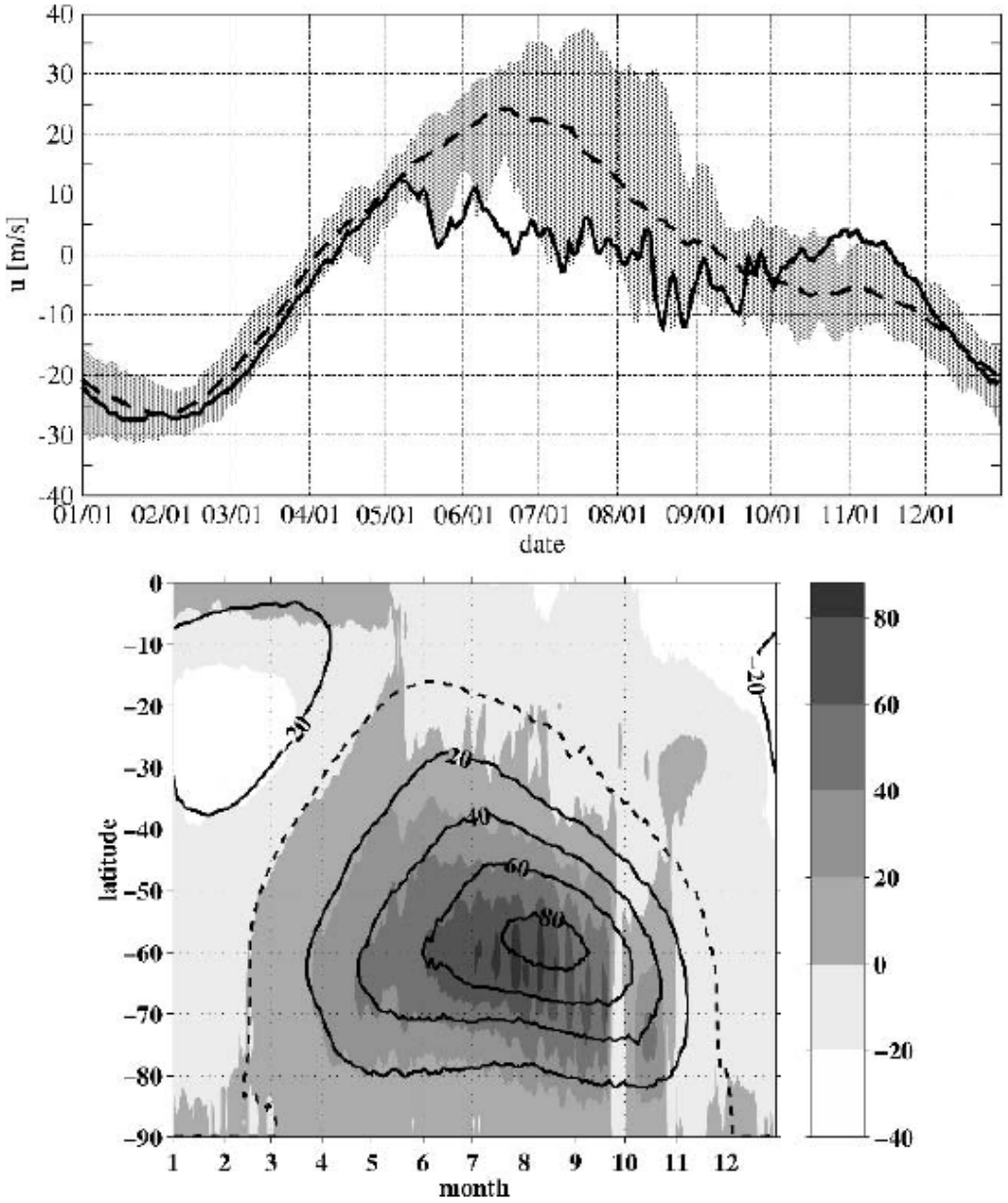

FIG. 3. (top) Time evolution of zonal-mean wind at 10 hPa, 30°S for 2002 (solid) and the 1979–2001 mean (dashed). The shading represents the range of observed values for 1979–2001. (bottom) Latitude–time plot (using daily data) of zonal-mean wind at 10 hPa (m s^{-1}). The 1979–2001 mean in contours (zero line dashed), where the 2002 mean is shaded, with negative values bright and positive values gray.

Seasonal climatology of wave geometry

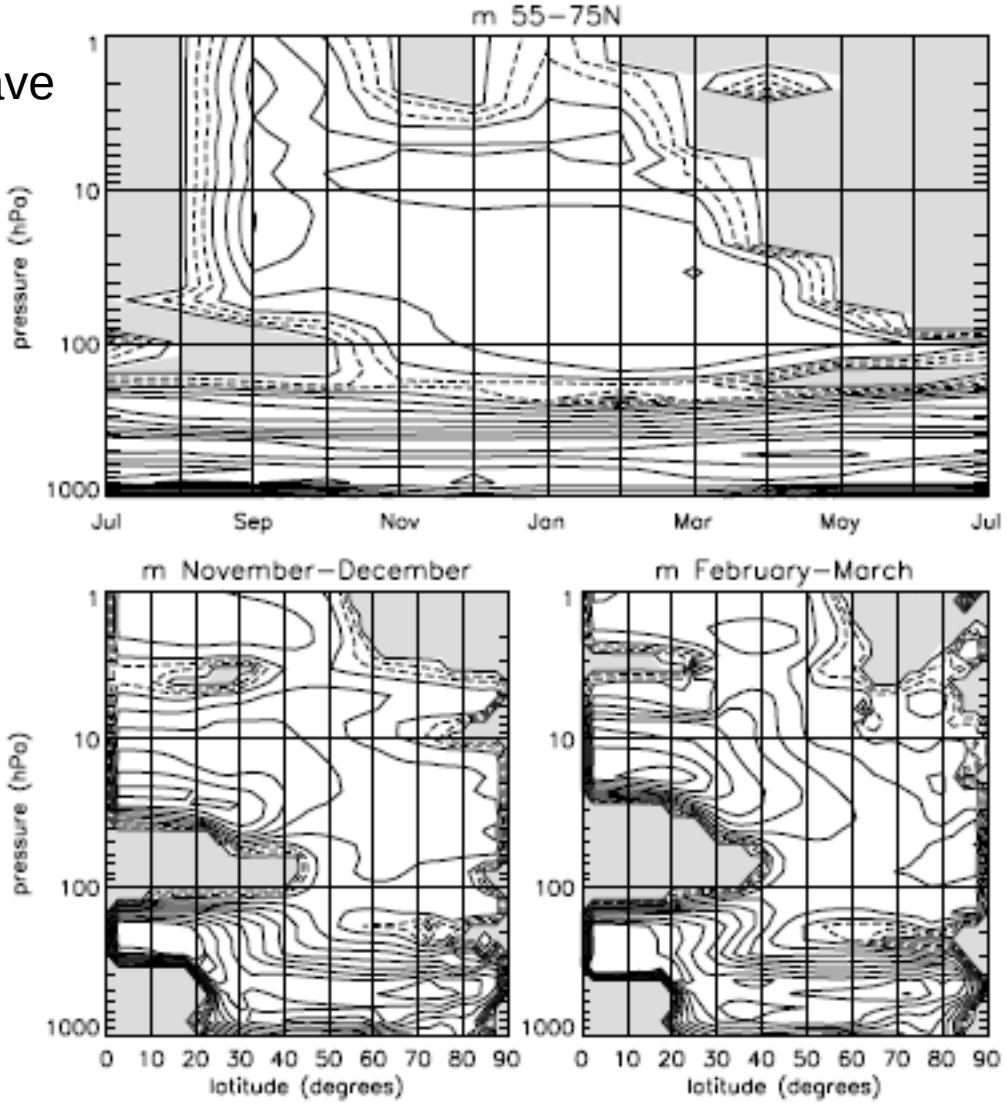

FIG. 8. The climatological seasonal cycle of the vertical wavenumber averaged between 55 and 75°N (top panel) and zonal-mean cross sections of the climatological vertical wavenumber in November-December (bottom left panel) and February-March (bottom right panel) in the northern hemisphere. Contours and shading as in Fig. 3.

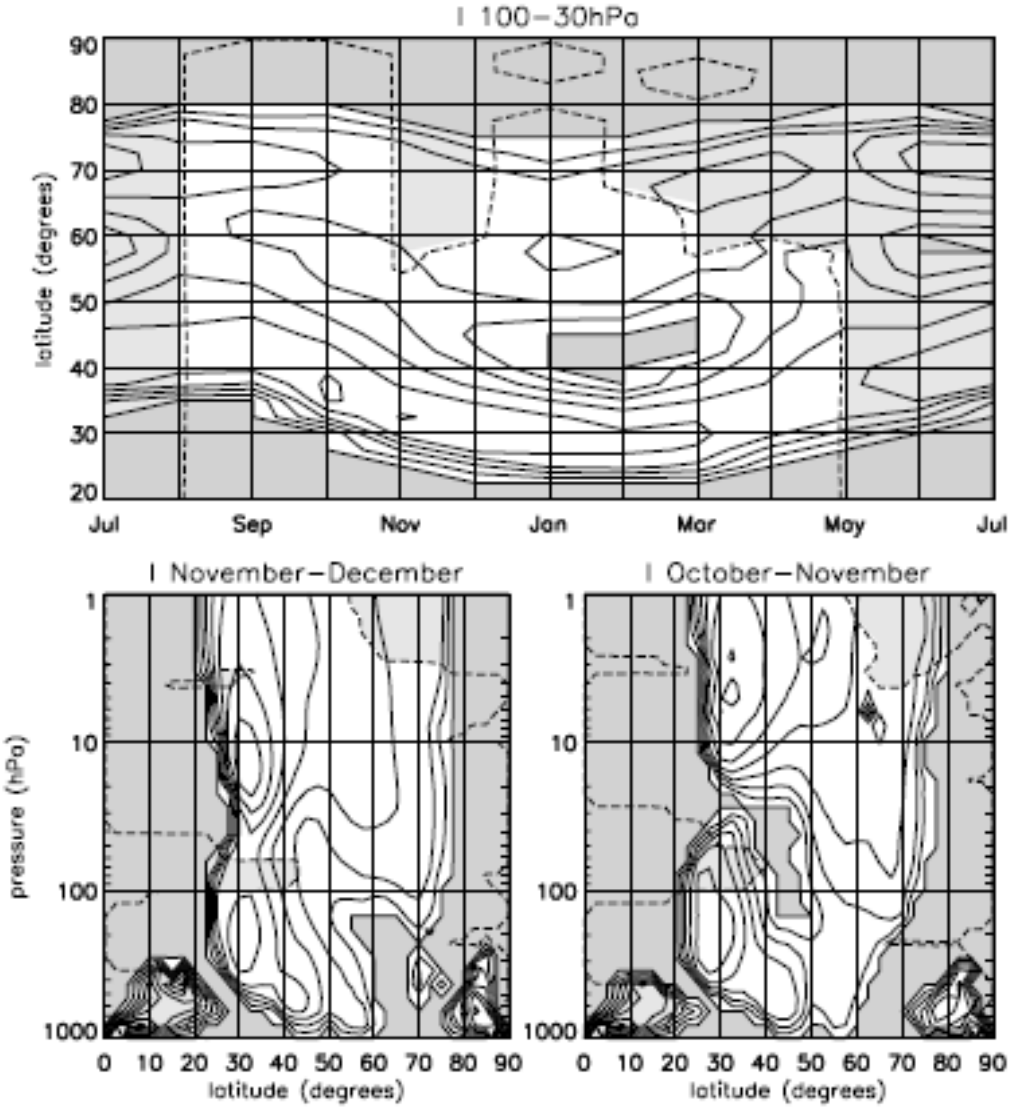

FIG. 9. The climatological seasonal cycle of the meridional wavenumber averaged between 100 and 30 hPa (top panel) and zonal-mean cross sections of the climatological meridional wavenumber in November-December (bottom left panel) and February-March (bottom right panel) in the northern hemisphere. Dark shading indicates regions of wave evanescence ($l < 0$). Overlying the climatological seasonal cycle of the meridional wavenumber is the seasonal cycle of the vertical wave number averaged between 3 and 1 hPa. The light shading indicates regions of wave evanescence ($m < 0$). Contours as in Fig. 4.

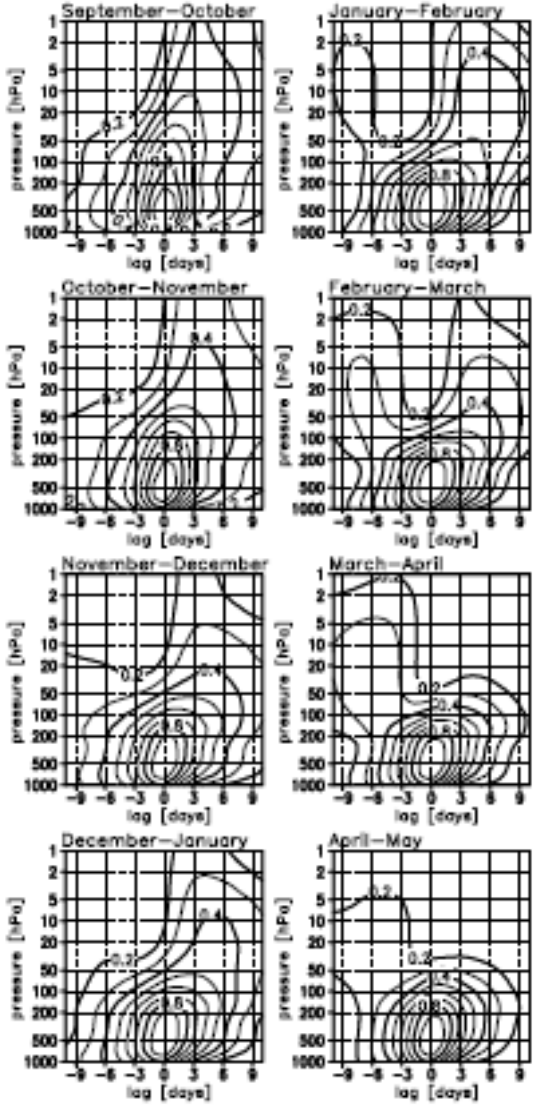

FIG. 6. Vertical-time lag section of the correlation coherence for wave one averaged from 45 to 80°N at 500 hPa with vertical levels between 1000 and 1 hPa for two-month overlapping periods from October-November to April-May and for time lags between -10 and 10 days. Contours and significance as in Fig. 1.

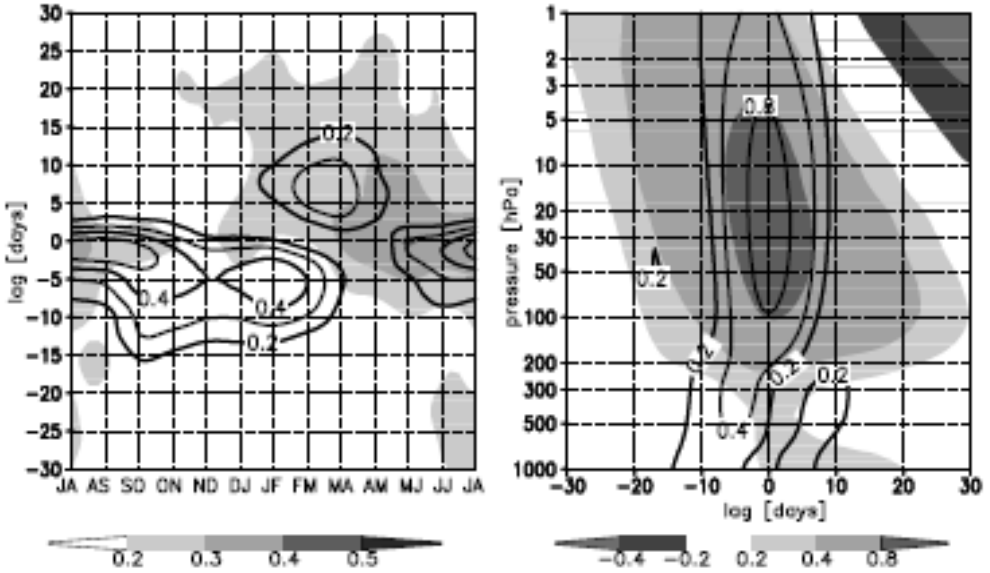

FIG. 12. The climatological seasonal cycle for two-month overlapping periods of the time-lagged correlation of the NAM index between 20 hPa and 1000 hPa (shaded) and the wave one cross-coherence correlations between 20 hPa and 500 hPa both averaged from 45 to 80°N (solid lines) for time lags between -30 and 30 days (left panel). The right panel shows the time-lagged correlation of the NAM index between 20 hPa and 1000 hPa (shaded) and the wave one cross-coherence correlations between 20 hPa and 500 hPa (solid lines) from December to March.

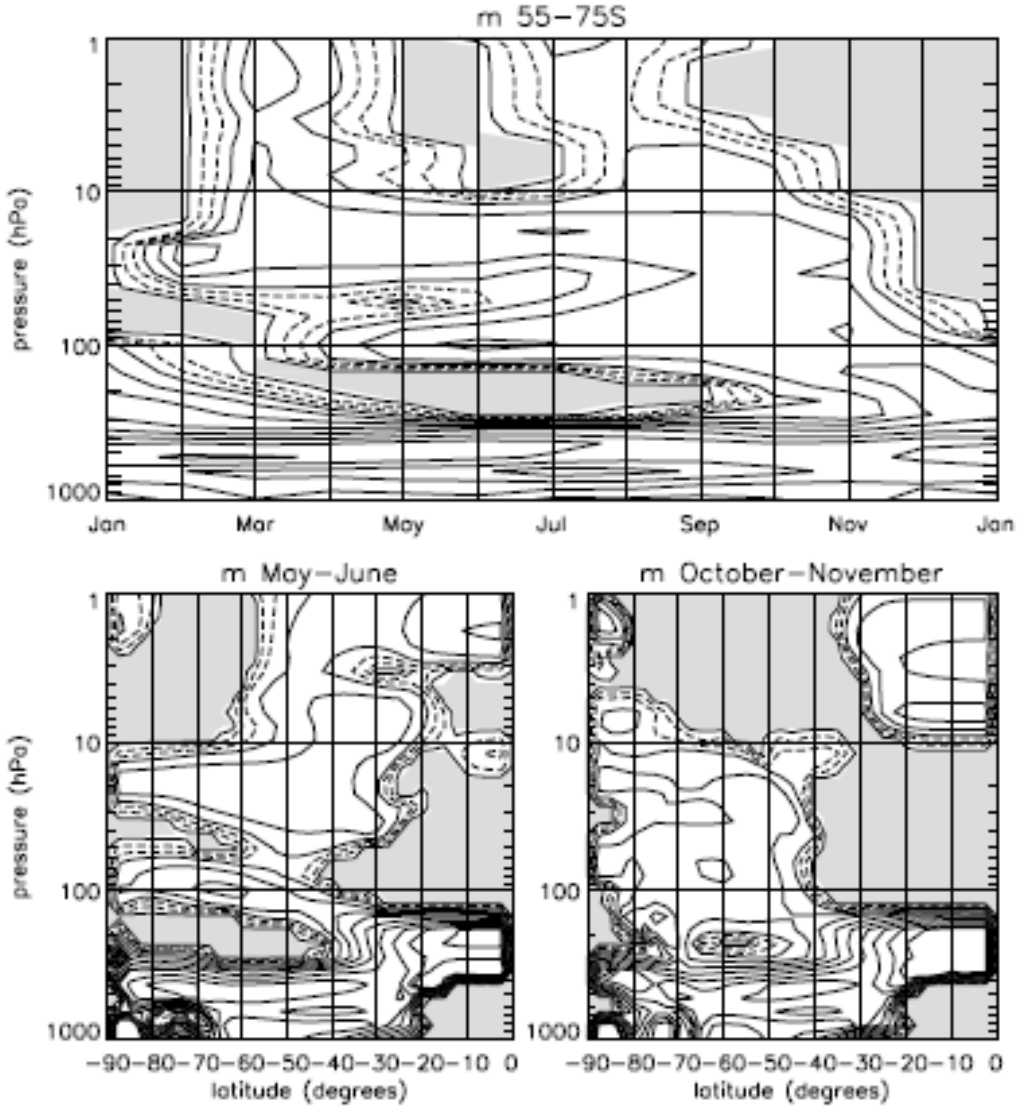

FIG. 3. The climatological seasonal cycle of the vertical wavenumber averaged between 55 and 75°S (top panel) and zonal-mean cross sections of the climatological vertical wavenumber in May-June (bottom left panel) and October-November (bottom right panel) in the southern hemisphere. The contours (units 10^{-5} m^{-1}) are shown at 0.01 (thick line); 2, 4 (dashed line); and 6-30 in jumps of 3 (solid). Shading indicates regions of wave evanescence ($m < 0$).

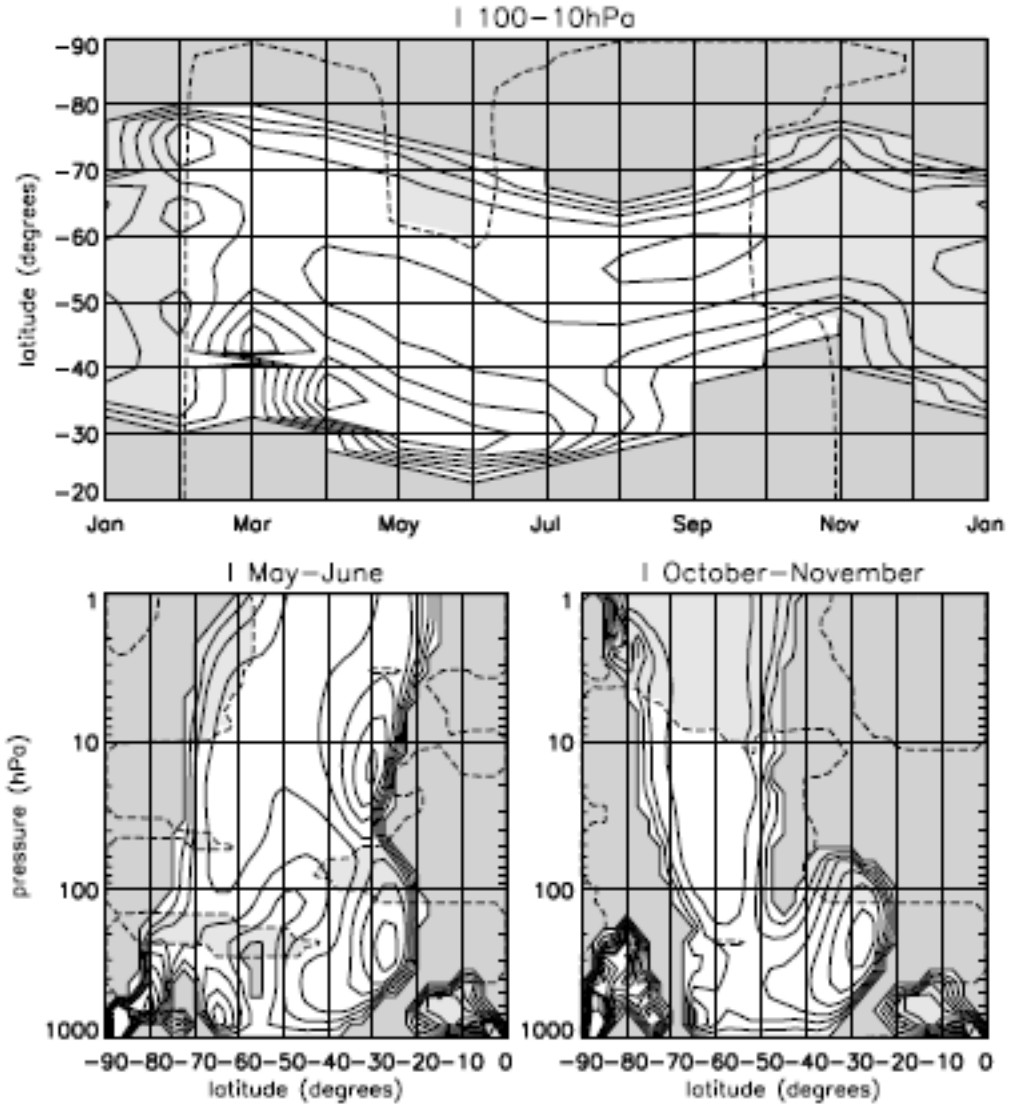

FIG. 4. The climatological seasonal cycle of the meridional wavenumber averaged between 100 and 30 hPa (top panel) and zonal-mean cross sections of the climatological meridional wavenumber in May-June (bottom left panel) and October-November (bottom right panel) in the southern hemisphere. The contours interval is 1 rad^{-1} and the thick line represents the 0.01 contour. Dark shading indicates regions of wave evanescence ($l < 0$). Overlying the climatological seasonal cycle of the meridional wavenumber is the seasonal cycle of the vertical wave number averaged between 10 and 1 hPa. The light shading indicates regions of wave evanescence ($m < 0$). The dashed line shows the $m = 0.01$ m^{-1} contour.

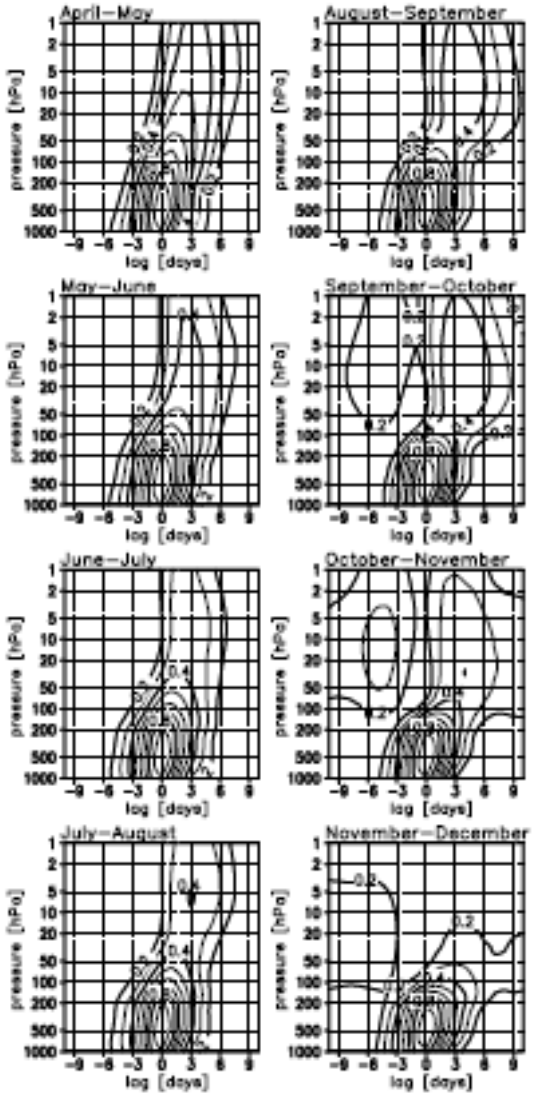

FIG. 1. Vertical-time lag section of the correlation coherence for wave one averaged from 45 to 80°S at 500 hPa with vertical levels between 1000 and 1 hPa for two-month overlapping periods from April-May to November-December and for time lags between -10 and 10 days. Only correlations which are statistically significant at the 99% levels are contoured and the contour interval is 0.1.

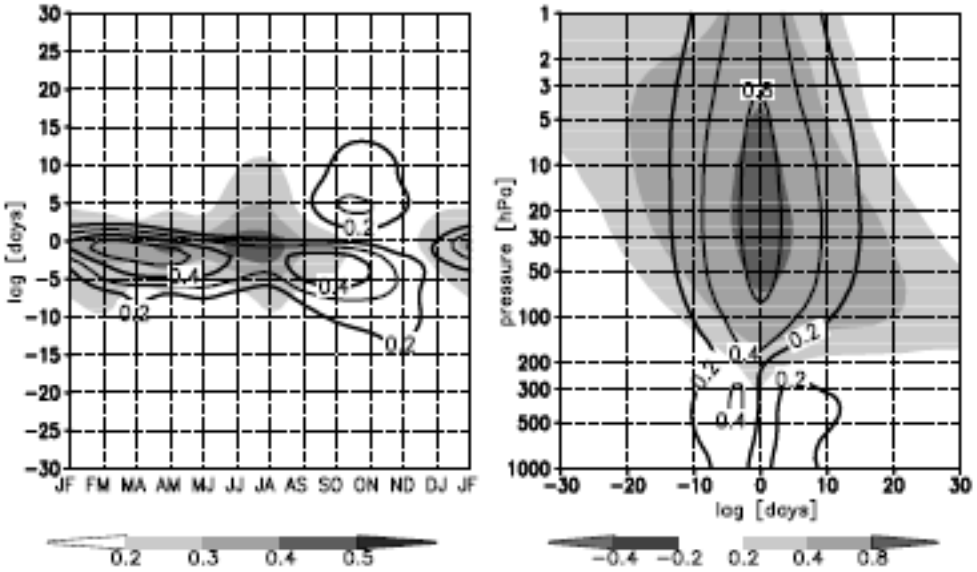

FIG. 11. The climatological seasonal cycle for two-month overlapping periods of the time-lagged correlation of the SAM index between 20 hPa and 1000 hPa (shaded) and the wave one cross-coherence correlations between 20 hPa and 500 hPa both averaged from 45 to 80°S (solid lines) for time lags between -30 and 30 days (left panel). The right panel shows the time-lagged correlation of the SAM index between 20 hPa and 1000 hPa (shaded) and the wave one cross-coherence correlations between 20 hPa and 500 hPa (solid lines) from September to December.

$$n_{\text{ref}}^2 \equiv \frac{N^2}{f^2}\left[\frac{\overline{q}_y}{U} - k^2 + F(\rho, N^2)\right] = m^2 + \frac{N^2}{f^2}l^2,$$

$$\overline{q}_y = \beta - U_{yy} + \frac{f^2}{N^2}\frac{U_z}{h} - \frac{f^2}{N^2}U_{zz} + f^2 U_z \frac{N_z^2}{(N^2)^2},$$

$$m^2 \approx \frac{N^2}{f^2}\beta + \frac{U_z}{h} - U_{zz}.$$

Southern hemisphere late winter- September- October:

TABLE 1. Statistical features of the 1 Sep–16 Oct 50°–70°N means of the 5–1-hPa mean m^2 (shown in Fig. 2d) and the 10–1-hPa means of U_{zz} (Fig. 3b), $\overline{q}_y$, N^2 (Fig. 3a), U_z, and U. Shown are the de-

	Correlation with $\langle m^2 \rangle$
$\langle m^2 \rangle$	**1.0**
$\langle U_{zz} \rangle$	**−0.73**
$\langle q_y \rangle$	**0.62**
$\langle N^2 \rangle$	**0.60**
$\langle U_z \rangle$	0.25
$\langle U \rangle$	**0.66**